UNIVERSITY OF GÄVLE

FACULTY OF ENGINEERING AND SUSTAINABLE DEVELOPMENT

Department of Building Engineering, Energy Systems and Sustainability Science

Measurements of solar radiation, development of a climate file for Gävle and calibration of a PV-simulation program

Author: Victor Hernando Uriarte

Year: 2024

Student thesis, Advanced level (Master degree, one year), 15 HE
Energy Systems
Programme: Master Programme in Energy Systems

Supervisor: Diogo O. Cabral
Assistant supervisor: Björn Karlsson
Examiner: Mathias Cehlin

Abstract

The research proposed consists in providing a climatic file of received radiation together with solar electric generation for a 1.17 kWp PV system in the city of Gävle. In addition, both radiation and solar electric generation will be compared making use of the WINSUN program. Possible disparities between both data have been analyzed. The interest of this study lies in the lack of a file that provides radiation data in the city of Gävle, which may be of help to people interested in making some kind of photovoltaic installation. Similar studies have been carried out previously in different locations which have tested different models to evaluate various climatic factors affecting the performance of the panels. The research method has been a case study in which monocrystalline solar panels installed in building 45 of the University of Gävle (HiG) have been analyzed together with the radiation data provided by three pyranometers. The results exhibit the importance of adjusting parameters such as diffuse coefficient, horizontal shading, and system efficiency. Results of this study show an accurate climate file, with little errors between measured and simulated data, with values of global performance indicator (GPI) (-2.70E-10, -1.06E-12) for 2022 and 2023 respectively.

Keywords: PV panels, comparison of measurement and simulation, photovoltaic, solar diffuse radiation, solar production, PV panels in Sweden.

Acknowledgements

First and foremost, I would like to express my gratitude to my supervisor, Diogo Cabral, for accepting my thesis and providing me with the invaluable opportunity to work alongside him. I would also like to extend my sincerest thanks to my assistant supervisor, Björn O Karlsson, for his unwavering effort, dedication, and kindness. His guidance and support have been instrumental in my professional development, and I am truly grateful for the insights he has imparted during this process. He has been able to share his passion for PV energy with me and encouraged me to learn more about the topic.

Furthermore, I would be remiss if I did not express my gratitude to my family, who have provided me with the opportunity to pursue my studies in Sweden and have consistently sought to ensure that my decisions align with my best interests.

In addition, I would like to acknowledge the invaluable support of the individuals I have had the privilege of meeting during this course, as well as the friends I hope to retain for the remainder of my life. Their guidance and encouragement have been instrumental in making this experience one of the most rewarding thus far.

In conclusion, this dissertation marks the conclusion of my academic career at the University of the Basque Country at the School of Engineering in Bilbao. I would like to express my gratitude to all the individuals I have encountered during these years, including fellow students, professors, and university staff. These years have been transformative, allowing me to grow not only physically and professionally, but also personally.

Table of contents

Abstract ii
Acknowledgements iii
List of Figures vi
List of Tables viii
Abbreviations and Acronyms ix
Nomenclature x
Greek x
Latin xi
1 Introduction 1
1.1 Background 1
1.2 Literature Review 2
1.3 Aims 4
1.4 Approach 4
2 Theory 5
2.1 Solar radiation 5
2.2 PV cells 5
2.2.1 PV cell technologies 6
2.3 PV installation components 8
2.3.1 Combiner box 8
2.3.2 PV disconnect switch 8
2.3.3 Charge controller 9
2.3.4 Battery 9
2.3.5 Inverter 9
2.3.6 System metering 10
2.3.7 Mounting systems 10
2.4 PV performance 11
2.4.1 Solar radiation 11
2.4.2 IV and PV curve 11
2.4.3 Types of radiation 12
2.4.4 Solar angles 14
2.5 WINSUN Equations 17
2.5.1 Calculation of the performance of a PV-system in WINSUN 17
3 Method 19
3.1 PV installation 19
3.1.1 Location 19
3.1.2 Solar panels 20
3.1.3 Inverter 20
3.1.4 Pyranometers 21
3.2 Data collection 22
3.2.1 Data logger 22
3.3 Climatic data 22
3.3.1 Temperature data 22
3.3.2 Snow data 23

3.4 WINSUN program 23
3.4.1 Input data 23
3.5 Diffuse radiation towards a horizontal surface $G_{d,h}$ 25
3.5.1 Processing of data entered into WINSUN in 2023 25
3.5.2 Processing of data entered into WINSUN in 2022 30
3.6 Comparison between $G_{45°/-12.5°}$ measured and simulated 33
3.7 Statistical comparison 34
3.8 Other sources for PV output 35
3.8.1 Photovoltaic Geographical Information System (PVGIS) 35
3.8.2 STRÅNG data entered into WINSUN program 35
3.8.3 WINSUN website 35
4 Results 36
4.1 Comparison of results with different data sources and solar production calculations softwares 36
4.1.1 Measured and simulated PV output comparison 36
4.1.2 Comparison with results obtained with PVGIS 38
4.1.3 Comparison with STRÅNG data entered into WINSUN program ..40
4.1.4 Comparison with WINSUN website results 41
4.1.5 Statistical errors of the results 42
4.2 Effect of altering the parameters 43
4.2.1 Effect of the diffuse acceptance coefficient Kd 43
4.2.2 Effect of the system efficiency 43
4.2.3 Effect of the horizontal shading 44
4.2.4 Most accurate model 44
4.3 Overall results 46
4.4 Different factors influencing the PV performance 47
4.4.1 Influence of the snow in the PV performance 47
5 Discussions 49
6 Conclusions 51
6.1 Study results 51
6.2 Outlook 51
6.3 Perspectives 52
References 53
Appendix A 1
Appendix B 1
Mean values 1
Mean Bias Difference (MBD) 1
Root Mean Square Difference (RMSD) 1
Coefficient of determination (R^2) 1
Expanded uncertainty (U_{95}) 1
T-statistic test (TT) 2
Global Performance Indicator (GPI) 2

List of Figures

Figure 1 Scheme of a PV cell when converting photon energy into electricity (Patel, 1999) .5
Figure 2 Formation of arrays in solar panels(Nabipour Afrouzi et al., 2013).....6
Figure 3 Monocrystalline solar cell (Monocrystalline Solar Cell and Its Efficiency - SolarSena, 2021.).....6
Figure 4 Polycrystalline solar cell (P Type Polycrystalline Silicon Solar Cell - China Polycrystalline Silicon and Poly Cell,2019.) 7
Figure 5 Thin film solar cell (Innovation: Thin Film Solar Cells at MX2016 - MaterialDistrict, 2016.) 7
Figure 6 Amorphous silicon solar cells (Types of Solar Panels: Types, Working, Application with (PDF), 2022).....7
Figure 7 Solar combiner box for 4 strings with 15A rated current(Solar Combiner Box PV Combiner Box 4 String With15A Palestine | Ubuy, 2018) 8
Figure 8 DC and AC switches in building 45 of the University of Gävle 8
Figure 9 Scheme of a solar panel with a Maximum Power Point Tracking (MPPT) charge controller and a battery (99% Efficiency 80A 100A MPPT Solar Charge Controller 48V/96V, 2019).....9
Figure 10 Picture of a generic inverter (Solar Inverters | SMA Solar, n.d.)..... 10
Figure 11 SMA Energy Meter (SMA Energy Meter EMETER-20 | Mg-Solar-Shop, 2020) 10
Figure 12 Mounting system for solar panels (Ground Static Mounting System for Solar Panels SMS-402 by SolarSK, n.d.)..... 11
Figure 13 Current voltage curve of a solar cell (IV Curve | PVEducation, 2019)..... 12
Figure 14 Graphical representation of beam, beam normal and beam horizontal radiation (Björn O Karlsson, 2022) 13
Figure 15 Representation of the declination angle δ together with the latitude λ (λ_l in figure) and longitud L..... 14
Figure 16 Description of the zenith angle, surface azimuth angle, solar azimuth angle for a tilted surface, and tilt (Duffie et al., 2020.)..... 16
Figure 17 Location of the study 19
Figure 18 PV-system of building 45 in the university of Gävle 20
Figure 19 SUNNY BOY 1200 inverter(Solar Technology, n.d.) 20
Figure 20 Pyranometers in building 45 measuring total radiation in a horizontal surface and in a tilted surface..... 21
Figure 21 Pyranometer with a shading ring taking diffuse radiation..... 21
Figure 22 Data logger Campbell Scientific CR 1000 (CR1000: Measurement and Control Datalogger, 2007.) 22
Figure 23 Location where temperature data was collected (Ladda Ner Meteorologiska Observationer | SMHI, n.d.)..... 23
Figure 24 Comparison between the $G_{d,h}$ and the G_h in 2023 in HiG (Measurements taken by the pyranometers 2 and 3) 26
Figure 25 Comparison between measured diffuse horizontal radiation and calculated one with Eq. 24 in 2023 27
Figure 26 Comparison of the measured diffuse horizontal radiation and the adjusted one in 2023 28
Figure 27 Comparison of the global horizontal radiation with the adjusted diffuse horizontal radiation in 2023..... 28
Figure 28 Monthly data for G_h, $G_{d,h}$, $G_{b,h}$ with raw data 2023 29

Figure 29 Monthly data for G_h, $G_{d,h}$, $G_{b,h}$ with adjusted data 2023 29
Figure 30 Comparison between the $G_{d,h}$ and the G_h in 2022 in the HiG (Measurements taken by the pyranometers 2 and 3) 30
Figure 31 Comparison between measured diffuse horizontal radiation and calculated one with Eq. 24 in 2022 30
Figure 32 Comparison of the measured diffuse horizontal radiation and the adjusted one in 2022 31
Figure 33 Comparison of the global horizontal radiation with the adjusted diffuse horizontal radiation in 2022 31
Figure 34 Monthly data for G_h, $G_{d,h}$, $G_{b,h}$ with raw data 2022 32
Figure 35 Monthly data for G_h, $G_{d,h}$, $G_{b,h}$ with adjusted data 2022 32
Figure 36 Comparison between $G_{45°/-12.5°}$ measured and simulated in 2022 33
Figure 37 Comparison between $G_{45°/-12.5°}$ measured and simulated in 2023 33
Figure 38 Difference between $G_{45°/-12.5°}$ measured and simulated in January and December 2022 34
Figure 39 Difference between G45°/-12.5° measured and simulated in January and December 2023 34
Figure 40 PV output comparison between 1.17 kW PV-system output and the simulation with WINSUN entering radiation data collected in Building 45 for 2022 36
Figure 41 PV output comparison between 1.17 kW PV-system output and the simulation with WINSUN entering radiation data collected in Building 45 for 2023 37
Figure 42 PV output comparison between 1.17 kW PV-system output in building 45 of the HiG and the simulation with PVGIS for 2022 39
Figure 43 PV output comparison between 1.17 kW PV-system output in building 45 of the HiG and the simulation with PVGIS for 2023 39
Figure 44 PV output comparison between 1.17 kW PV-system output in building 45 of the HiG and the simulation with STRÅNG data entered into WINSUN for 2022 40
Figure 45 PV output comparison between 1.17 kW PV-system output in building 45 of the HiG and the simulation with STRÅNG data entered into WINSUN for 2023 41
Figure 46 PV output comparison between 1.17 kW PV-system output in building 45 of the HiG and the simulation with WINSUN data for 2022 41
Figure 47 PV output comparison between 1.17 kW PV-system output in building 45 of the HiG and the simulation with WINSUN data for 2023 42
Figure 48 Comparison between measured and simulated data after adjusting parameters 2022 45
Figure 49 Comparison between measured and simulated data after adjusting parameters 2023 46
Figure 50 Snow depth and PV output representation for years 2022 and 2023 47
Figure 51 Snow depth and PV output representation together with total radiation with a β = 45° for years 2022 and 2023 48
Figure 52 Solar panels covered by snow in the PV system of HiG 48

List of Tables

Table 1 PV input data for the studied localization..... 24
Table 2 Characteristics of the PV modules 24
Table 3 Detail input data for the PV modules..... 25
Table 4 PV output comparison between 1.17 kW PV-system output and the simulation with WINSUN entering radiation data collected in Building 45 for 2022..... 37
Table 5 PV output comparison between 1.17 kW PV-system output and the simulation with WINSUN entering radiation data collected in Building 45 for 2023..... 38
Table 6 Statistical errors of the estimations of PV solar production in the building 45 of the HiG in 2022 42
Table 7 Statistical errors of the estimations of PV solar production in the building 45 of the HiG in 2023 43
Table 8 Statistical errors of the estimations of PV solar production in the building 45 of the HiG in 2022 changing Kd 43
Table 9 Statistical errors of the estimations of PV solar production in the building 45 of the HiG in 2023 changing Kd 43
Table 10 Statistical errors of the estimations of PV solar production in the building 45 of the HiG in 2022 changing system efficiency 44
Table 11 Statistical errors of the estimations of PV solar production in the building 45 of the HiG in 2023 changing system efficiency 44
Table 12 Statistical errors of the estimations of PV solar production in the building 45 of the HiG in 2022 changing horizontal shading..... 44
Table 13 Statistical errors of the estimations of PV solar production in the building 45 of the HiG in 2023 changing horizontal shading..... 44
Table 14 Statistical errors of the estimations of PV solar production in the building 45 of the HiG in 2022 changing three parameters 45
Table 15 Statistical errors of the estimations of PV solar production in the building 45 of the HiG in 2023 changing three parameters 45
Table 16 Overall results for 2022..... 46
Table 17 Overall results for 2023..... 47

Abbreviations and Acronyms

Letters	Description
AC	Alternate Current
AM	Air Mass
DC	Direct Current
DTU	University of Denmark
GPI	Global Performance Indicator
HiG	University of Gävle
IEA	International Energy Agency
IR	Infra-red radiation
MBD	Mean Bias Difference
MPPT	Maximum Power Point Tracking
PV	Photovoltaic
PVGIS	Photovoltaic Geographical Information System
R^2	Coefficient of determination
rMBE	Relative Mean Bias Error
RMSD	Root Mean Square Difference
SD	Standard Deviation
SMHI	Swedish Meteorological and Hydrological Institute
STC	Standard Test Conditions
TT	T-statistic Test
UV	Ultraviolet radiation
Uxx	Expanded Uncertainty
VIS	Visible light radiation

Nomenclature

Greek

Symbol	Description	Unit
α	coefficient for temperature dependence of PV-module	1/K
α_s	Solar altitude angle	°
β	Tilt angle	°
δ	Declination	°
ε	Emissivity factor	-
η	Efficiency	-
θ	angle of incidence for a tilted surface	°
θ_z	zenith angle	°
λ	Latitud	°
ρ_g	Reflectance of the ground	-
σ	Stefan-Boltzmann's constant	$W/(m^2 K^4)$
ω	hour angle	°
γ	Surface azimuth angle	°
γ_s	Solar azimuth angle	°

Latin

Symbol	Description	Unit
A_i	Anisotropic index	-
$A_{PV\text{-}SYSTEM}$	Area of the solar panels of the PV-system	m^2
F_d	Diffuse fraction	-
G	Total radiation	W/m^2
G_b	Beam radiation	W/m^2
$G_{b,h}$	Beam radiation towards horizontal surface	W/m^2
$G_{b,n}$	Beam radiation towards perpendicular surface	W/m^2
G_d	Diffuse radiarion	W/m^2
$G_{d,h}$	Diffuse radiation towards horizontal surface	W/m^2
G_g	Ground reflected radiation	W/m^2
G_h	Total radiation towards horizontal surface	W/m^2
$G_{o,n}$	Radiation outside the atmosphere towards a perpendicular surface	W/m^2
G_{sc}	Solar constant	W/m^2
h	Heat transfer coefficient	$W/(m^2 K)$
hh	Hours	°
I_{MP}	Maximum power current	A
I_{sc}	Short circuit current	A
K_b	Correction factor for direct irradiation	-
K_d	Correction factor for diffuse irradiation	-

L	Longitud	º
L_l	longitude of the location	º
L_s	Standard meridian for the local time zone	º
mm	minutes	‘
n	day number of the year	day
n_0	thermal solar absorption of the PV modules	-
p	Angular dependent coefficient	-
P	Power	W
P_{MP}	Maximum power	W
Q	Radiated power per surface area	W/m^2
R	Geometry factor	-
T	Temperature	K-ºC
$T_{ambient}$	Ambient temperature	ºC
T_{cell}	Temperature of the cell	ºC
V_{MP}	Maximum power voltage	V
V_{oc}	Open circuit voltage	V

1 Introduction

1.1 Background

Within the global energy context, we find ourselves at a time when renewable energies are taking on a relevant role. This is mainly due to the Paris treaty adopted by 196 parties in 2015, which aims to limit the increase in global temperature to 1.5 ºC above pre-industrial levels. This study will be carried out in Gävle, Sweden, a country which in recent years has experienced a large increase in the share of renewable energies in its energy mix to almost 60% by 2020 according to the International Energy Agency (IEA).

According to the IEA solar photovoltaic (PV) generation increased up to 1300 TWh in 2022, increasing 26% respecting to the previous year, which means that it has been the fastest growing renewable energy surpassing wind energy.

China has been a major player in the increase of this type of energy generation, accounting for 38% of PV generation, followed by United States with 15%. The fact that the two major world powers are betting on this technology makes its potential much greater (*Solar - IEA*, 2023).

In the Swedish energy mix, photovoltaic solar energy does not form a large share. This technology has not been developed as much in this country for obvious reasons, such as the low radiation received, and the few hours of sunshine compared to other countries located at lower latitudes. However, this does not mean that this type of installations are not profitable. On the other hand, the large hydroelectric capacity of the country, and the extension for the installation of wind turbines have also caused a lower development of solar photovoltaic energy.

The interest of this work resides in the scarce offer of climate archives that can provide joint data of received radiation together with solar electric generation in the city of Gävle. This will facilitate the installation of a larger number of PV solar panel installations.

When a prospective customer asks several companies about the potential for a PV installation at his home, he receives different values because the companies use different sources to determine the radiation at each location. With this climate file, prospective customers will be able to compare offers based on the potential of the solar panels provided by the companies and possible variations due to different sources of irradiation data will not affect the results.

In addition, it will allow a better understanding of the technology of photovoltaic solar panels and what kind of circumstances affect their performance. These conclusions can be obtained because the data obtained belong to the production of photovoltaic panels will be compared with radiation data obtained from three pyranometers.

The objectives of this study are, as mentioned above, to provide data on the radiation received at the municipality of Gävle, to learn how photovoltaic panels work more precisely, what factors can affect their performance, and to compare radiation data with energy data obtained directly from the photovoltaic panels using the WINSUN program.

The topic of this study was proposed by my supervisor due to the lack of such study, which made me accept it directly because of my long-standing interest in renewable energies and in particular, solar PV energy.

1.2 Literature Review

Once the topic of this thesis has been decided as well as the principal objectives, literature research has been conducted to increase the knowledge in the field and to find answers to the questions that may have appeared. For this research, different browsers have been used such as, Discovery (HiG's meta search engine) and Google Scholar. With the aim to focus the research the following keywords have been used: "PV installations AND Sweden", "photovoltaic panels AND performance OR analysis", "evaluation AND PV systems" and "Solar panels AND pyranometers". Regarding the selected articles, it has been decided to include the most relevant peer-reviewed articles and those most related to the topic of study.

Considering that throughout this work a comparison will be made between data obtained directly from photovoltaic generation and data collected with three pyranometers, similar studies have been sought. Within the models that have been used for data comparison, relative mean bias error (rMBE) values from 0 to 8% have been obtained between the measured data and the calculated data. These results were obtained in a study located in Poland where data was collected from a database which had been gathering data with a pyranometer in a location 10 km away from where the place of measurements (Olczak, 2022).

Another study that provided a comparative analysis between theoretical values of insolation and actual measurements taken by pyranometers installed in solar photovoltaic plants was performed in the city of Dushanbe (Tajikistan). This study showed a discrepancy between both data, it oscillated between 1 and 20% depending on the season, which can be associated with dustiness, an important factor that must be taken into account(Kudusov et al., 2021).

Different factors can affect PV solar panels performance, being dust one of the factors that may reduce by 50% the performance of a PV solar panel, what highlights the importance of cleaning them regularly. This statement was done after doing research and evaluating different articles that were showing the impact dust had in different locations in Northern Africa(Rezvani et al., 2022). The difference between the locations where the dust effect on PV panels has been studied and the location where the measures of this theses will be carried out could lead one to believe that this data is irrelevant. However, snow is an important factor that should be taken into consideration due to the location of the study and could have similar effects to dust on the performance of PV solar panels.

Taking into consideration that the location of the PV installation is Gävle (Sweden) it is important to know how snow can affect to the power generation, since it is said that snow conditions con cause an average reduction of the generated electricity of 14.7%. Moreover, it was stated that snow removal agents can enhance an improvement in the performance of PV panels by 0.1–2.3%. These results were obtained after creating a new model designed for high-latitude regions which was predicting the best PV installation angles maximizing the PV power generation making use of weather data from the years 2012 to 2021 in which three different scenarios were carried out, one considering just precipitation and clouds, the second one considering snowfall, cover and melting and the third one having a snow-dissolving agent (Ruan et al., 2024).

A recent study in the city of Vasterås (Sweden) conducted research to know the potential of roof-mounted solar photovoltaic projects of this city. This analysis was undertaken using geographical information with energy system modeling technics, obtaining data from Lantmateriet, a swedish land survey. The results after evaluating three different scenarios displayed that "*5.74 km^2 usable area in Vasterås gives potential installed capacity as 727 MW$_p$, 848 MW$_p$, and 956 MW$_p$, and potential yearly electricity generation as 626 GWh, 720 GWh, and 801 GWh on pitched roofs and flat roofs with three scenarios, respectively*". Although Gävle's population and urban area is not as big as Vasterås' the difference is not very large and these numbers give an idea of how much potential for electricity production from solar panels a city like Gävle can have (Yang et al., 2020).

Since the main part of the work is to validate the estimated results with the data received by the pyranometers, it is important to know which methods can be used for comparison. The work carried out by (Stone, 1993) proposes the use of the t-statistic method for the evaluation and comparison of radiation estimation models. The work shows how the use of Mean Bias Difference (MBD) and Root Mean Square Difference (RMSD) separately can lead to the approval of an incorrect model. For this reason, the use of the t-statistic is recommended as this way the model will be evaluated in a more reliable way.

In order to compare the values of the measured data of solar radiation and the data obtained with simulation, some statistical methods will be utilized. In a study carried out in Algeria (Behar et al., 2015) an accurate model of prediction of direct solar power was studied. Using seventeen different models with the aim of estimating the performance of solar power projects where some meteorological data is not available. For the purpose of finding the best model, a new statistical factor was used in the work, the so-called Global Performance Indicator (GPI) which takes into account five different statistical factors. Among these statistical indicators, MBD, RMSD, Expanded Uncertainty (Uxx) being xx the confidence level, T-statistic test (TT) and coefficient of determination (R^2) were used. This statistical method will be used to validate the data and to differentiate the influence of different input data on the results.

It is of interest to know what kind of models could be used for the estimation of horizontal diffuse radiation. In a study carried out in Algeria (Jamil & Akhtar, 2017), sixteen empirical models for determining this value were studied and analyzed using the statistical method used in (Behar et al., 2015). The Model 3 (cubic model) resulted to be the best model out of the Category 1 (representing ratio between diffuse and global radiation) and validation data set (data to test the models).

In a study carried out by (Formolli et al., 2021) three cases in Norway, three cases in Sweden, and four cases in Denmark were evaluated. Technical aspects were considered such as estimation of solar potential and energy generation. On the other hand, non-technical aspects were exposed. Among these, findings show that municipalities have a vital role as well as the use of indicators to evaluate the performance of masterplans, analogue and digital tools for the performance of solar simulations, to be able to increase the awareness among the stakeholders.

Once research has been conducted on studies related to the research to be carried out, it is known which factors may affect the results obtained, and to what extent differences between the power generation of the solar panels and the results obtained using the data provided by the pyranometers are valid. Different ways of analyzing data have also been revealed. In addition, it has been seen the great potential of photovoltaic installations in Gävle, so the realization of this thesis is important to increase the solar electricity production in this city, thus reducing CO_2 emissions.

1.3 Aims

The overall aim of this project is, as mentioned above, to provide a climate file of received radiation and solar electric generation in the city of Gävle. To achieve this objective, a correction method will be used for the horizontal diffuse radiation data, performing calculations, and taking into account the data collected with the pyranometers. In addition, the extent to which different factors may affect the results will be studied. Another sub-objective of this project is to learn how to use the WINSUN program and what kind of calculations are performed in it.

One of the limitations of this project is that the data obtained is only for the last three years, from April 2021 to February 2024, and just data for 2022 and 2023 will be used since are the only two years for which complete annual data are available. Therefore, although it is a considerable range of years, it is not a very wide range so that certain climatic variations suffered during these years could affect the results obtained.

Moreover, the study will be carried out with pyranometers and specific photovoltaic panels, which have been installed for some time and may have suffered some deterioration over the years which could affect the recollected data.

1.4 Approach

Data for this thesis has been acquired from HiG solar laboratory, which comprise global, and diffuse radiation. In order to analyze the data, WINSUN program was used. The WINSUN program gives monthly PV energy production after entering hourly global and diffuse radiation as well as temperature data. The data fed into WINSUN was analyzed using different statistical methods with the goal of finding the most accurate approximation between measured and simulated data.

2 Theory

2.1 Solar radiation

Photovoltaic energy is the energy produced by converting sunlight into electricity using a technology based on the photoelectric effect. This transformation takes place in devices called photovoltaic panels. In photovoltaic panels, solar radiation excites the electrons of a semiconductor device, generating a small potential difference.

Although the photovoltaic effect has been known since the 19th century, it was in the 1950s, at the height of the space race, when photovoltaic panels began to undergo significant development. Initially used to supply electricity to geostationary communications satellites, they are now a renewable power generation technology (APPA Renovables,2022.).

Currently, there are different types of materials that can be used as PV cells, but the ones that are commercially important are solid semiconductors that form p-n (positive-negative) junction when solar energy falls.

Sunlight strikes the semiconductor material and it is excited, a flow of electrons is attracted across the junction by the electric field that is created when the p-n junction is formed. If the semiconductor p-n junction is connected to an external circuit, the flow of electrons produces direct current (DC) electricity ('Jenkins & 'Ekanayake, 2017).

2.2 PV cells

The roots of PV cells are similar to those of the classic p-n junction diode. In Figure 1 a scheme of how electricity is generated in the PV cell is shown. When the junction absorbs the solar light, the electron system of the material receives the energy of the photons, creating charge carriers that separate at the junction.

Electron-ion pairs in a liquid electrolyte or electron-hole pairs in a solid semiconductor material can be charge carriers. A potential gradient is generated by the charge carriers in the junction region, electrons are accelerated under the electric field and flow as current through an external circuit. The power converted to electricity is the resistance multiplied by the square of the current. The remaining photon power is the responsible for raising the temperature of the cell (Patel, 1999).

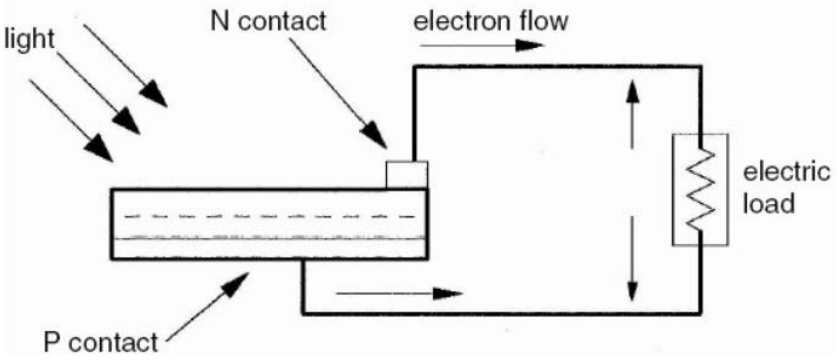

Figure 1 Scheme of a PV cell when converting photon energy into electricity (Patel, 1999)

The PV cell forms only a small part of the PV solar panel, which is only capable of producing about 1 watt of power. To produce more power, these cells are connected in series and in parallel to form so-called modules. In the same way these modules can be joined together to form arrays as we can see in Figure 2 (Patel, 1999). The negative part of the module is connected to the positive part of the next module. This connection adds the voltages, forming a string with much higher power. When one or more strings are added, they form an array with a current equal to the sum of the strings' currents (Franklin, 2018).

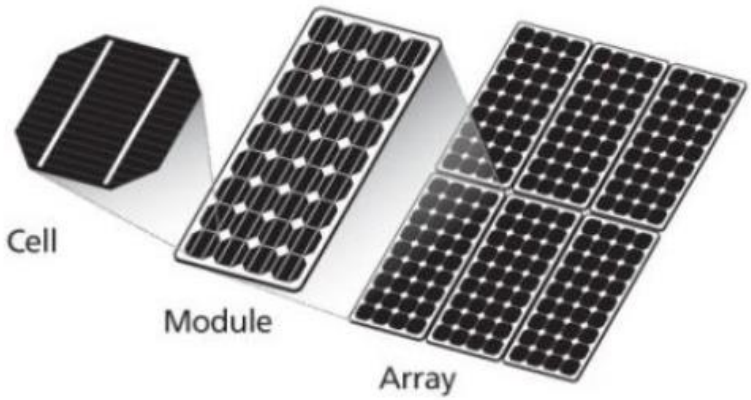

Figure 2 Formation of arrays in solar panels(Nabipour Afrouzi et al., 2013)

2.2.1 PV cell technologies

The goal of improving energy efficiency over time has led to the development of a wide variety of materials for solar panels. The following sections will describe the most common types of solar cells. Eq. 1 shows how efficiency (η) is calculated, its values vary among these different technologies.

$$\eta = \frac{output\ from\ the\ system}{radiation\ that\ arrived\ to\ the\ system} \qquad Eq.\ 1$$

2.2.1.1 Monocrystalline silicon

The monocrystalline silicon panels are made from melted and purified silicon. A seed crystal is placed in the liquid silicon and pulled at a slow speed (Patel, 1999). Efficiency of monocrystalline solar cells varies between 21 and 26.7%. Figure 3 is an illustration of what a monocrystalline solar cell looks like.

*Figure 3 Monocrystalline solar cell (*Monocrystalline Solar Cell and Its Efficiency - SolarSena*, 2021.)*

2.2.1.2 Polycrystalline silicon

Polycrystalline silicon is molten silicon poured into a square mold. It is simpler and less expensive than the monocrystalline silicon cell. (Gaikwad, 2020). Its efficiency varies between 13 and 16%. Figure 4 is an illustration of what a polycrystalline solar cell looks like.

*Figure 4 Polycrystalline solar cell (*P Type Polycrystalline Silicon Solar Cell - China Polycrystalline Silicon and Poly Cell*, 2019.)*

2.2.1.3 Thin film

Thin film solar cells are made of one or more layers of glass, metal, or plastic. Its efficiency varies between 21.7 and 23.4% (Gaikwad, 2020). Figure 5 illustrates how a thin film solar cell looks like.

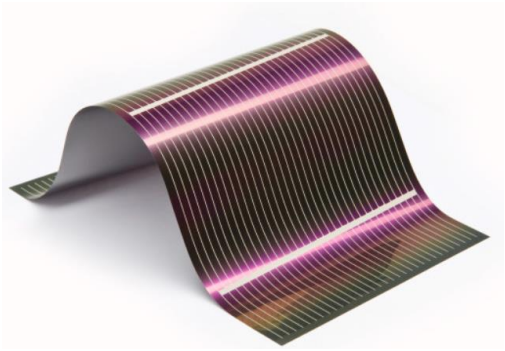

*Figure 5 Thin film solar cell (*Innovation: Thin Film Solar Cells at MX2016 - MaterialDistrict*, 2016.)*

2.2.1.4 Amorphous silicon

Amorphous silicon solar cells are a non-crystalline allotropic form of silicon and a well-developed technology used in small-scale applications. Its efficiency varies between 8.8 and 10.2% (Gaikwad, 2020). Figure 6 illustrates how an amorphous silicon solar cell looks like.

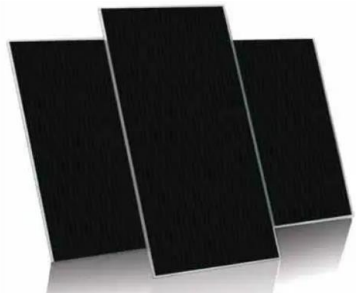

*Figure 6 Amorphous silicon solar cells (*Types of Solar Panels: Types, Working, Application with (PDF)*, 2022)*

2.3 PV installation components

2.3.1 Combiner box

The main function of the combiner box consists in combining the multiple series strings into a one parallel circuit. Once the strings are combined the voltage of the system remains the same as the one of each of the strings, but currents are added. The positive lead is connected to the fuse while the negative is connected to the rounded buss bar(Franklin, 2018). Solar combiner boxes are also responsible of consolidate the incoming power into one feed to distribute it to the inverter (What Is a Combiner Box? 2015).The combiner box is connected between the solar panels and the inverter. Figure 7 shows a combiner box of 4 strings, where is easy to differentiate between the input of the positive and negative part of the strings.

*Figure 7 Solar combiner box for 4 strings with 15A rated current(*Solar Combiner Box PV Combiner Box 4 String With15A Palestine | Ubuy*, 2018)*

2.3.2 PV disconnect switch

A PV disconnect switch must be installed as a DC disconnect switch between the inverter and the solar array. Its purpose is to de-energize and isolate the inverter from the power source. As per the electrical code, the negative conductors should be grounded while the positive ones should remain ungrounded.

A disconnect switch for PV is placed in the alternate current (AC) area before the AC service panel. Its function is to isolate the inverter from the AC service panel when the PV system is connected to the grid(Franklin, 2018). Figure 8 shows both DC and AC switches connected to the inverter in the building 45 of the university of Gävle where the case study has been carried out.

Figure 8 DC and AC switches in building 45 of the University of Gävle

2.3.3 Charge controller

If a battery is part of the PV system, a solar charge controller should also be part of the system. The purpose of the charge controller is to regulate the amount of energy flowing to the battery to prevent overcharging. During the day, the controller allows the PV array to charge the battery fully. At night, it is responsible for allowing the battery to power the load when energy is needed (Franklin, 2018).

Figure 9 illustrates the appropriate location for installing a solar controller. The solar controller receives DC input and delivers DC output based on the systems' requirements.

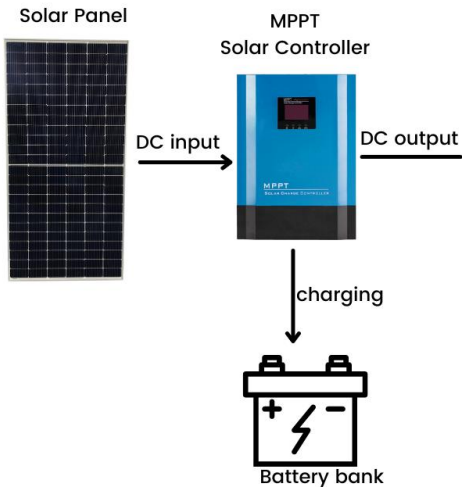

*Figure 9 Scheme of a solar panel with a Maximum Power Point Tracking (MPPT) charge controller and a battery (*99% Efficiency 80A 100A MPPT Solar Charge Controller 48V/96V*, 2019)*

2.3.4 Battery

The battery is responsible for storing excess energy in a PV system and supplying it when needed. If a single battery's voltage is insufficient, multiple batteries can be connected in series to increase voltage. It is important to design the battery bank based on the specific characteristics of the PV system. Another consideration is the life cycle of the product and its profitability for installation (Franklin, 2018).

2.3.5 Inverter

The inverter handles the conversion of DC to AC in a PV system. The DC can come directly from the PV panels or from the batteries. In residential settings, power loads operate in AC, which is why electricity needs to be converted into AC. The inverter's characteristics depend on those of the PV system. The inverter is also in charge of synchronizing the voltage and the frequency to the one of the electric grid. Moreover, it is responsible for controlling the energy flows, controlling efficiently when the energy is to be taken from the PV panels, from the batteries or from the grid.

Figure 10 portrays a generic inverter, in this case corresponding to one of the SMA Solar inverters that will be used in this case study.

*Figure 10 Picture of a generic inverter (*Solar Inverters | SMA Solar*, n.d.)*

2.3.6 System metering

PV installations should be equipped with system metering devices to measure the amount of electricity used from the PV system. It is also important to monitor the frequency of battery charging and discharging to identify any issues related to incomplete charging or system shutdown. Customers can track their consumption and electricity production data using various well-designed apps. Smart meters and data loggers are utilized for these practices (Franklin, 2018). Figure 11 illustrates an example of an energy meter used for PV installations.

*Figure 11 SMA Energy Meter (*SMA Energy Meter EMETER-20 | Mg-Solar-Shop*, 2020)*

2.3.7 Mounting systems

Solar panel mounting systems are crucial for maximizing solar energy generation. They provide the most advantageous orientation for solar panels towards the sun. These systems provide the structure for installing solar panels. The two typical options for installing mounting systems are roof-mounting and ground-mounting (*Solar Panel Mounting Systems: Types and Considerations for Installers*, 2023).

*Figure 12 Mounting system for solar panels (*Ground Static Mounting System for Solar Panels SMS-402 by SolarSK, *n.d.)*

2.4 PV performance

2.4.1 Solar radiation

In order to explain the theory of PV solar performance a brief explanation will be done regarding the solar radiation topic.

The solar constant G_{sc} is the energy from the sun per unit of time received on a unit area of surface perpendicular to the direction of propagation of the radiation at mean earth-sun distance outside the atmosphere. The solar constant has an average value of 1367 W/m^2.

Solar radiation can be divided into three different parts:

Ultraviolet radiation (UV): wavelength (λ) < 0.38 µm

Visible light (VIS): 0.38 µm < λ< 0.78 µm

Infra red radiation (IR): λ > 0.38 µm

The intensity and the spectral distribution of the solar radiation looks like the radiation from a black body at about 6000 K. A so-called black body is a body with emittance, $\varepsilon = 1$, in Stefan-Boltzmann's law valid for all bodies:

$$Q = \varepsilon\sigma T^4 \qquad \textit{Eq. 2}$$

Q = radiated power per surface area (W/m^2)

ε = emissivity factor or emittance

σ = Stefan-Boltzmann's constant = $5.67*10^{-8}$ W/m^2K^4

T = temperature of the body (K) (Duffie et al., 2020)

2.4.2 IV and PV curve

The IV and PV curves show the performance of each of the PV modules which are represented in Figure 13.

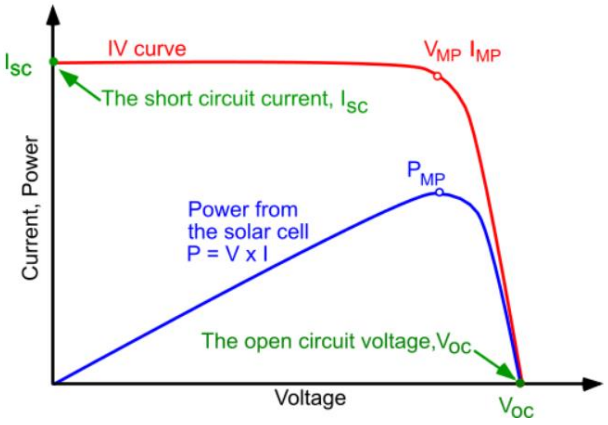

*Figure 13 Current voltage curve of a solar cell (*IV Curve | PVEducation*, 2019)*

Some important values of solar modules are represented in Figure 13.:

I_{sc} : Short circuit current, represents the maximum current of solar module.

I_{MP}: Maximum power current represents the current operating at maximum power.

V_{oc}: Open circuit voltage represents the maximum voltage of a solar module.

V_{MP}: Maximum power voltage represents the voltage operating at maximum power.

P_{MP}: Maximum power represents the maximum power a solar module is able to deliver.

2.4.3 Types of radiation

2.4.3.1 Calculation of beam radiation

Beam radiation G_b: Corresponds to the solar radiation received from the sun without taking into consideration the scattered radiation by the atmosphere.

Diffuse radiation G_d: Corresponds to the solar radiation received from the sun that has been scattered by the atmosphere and it is not directly impacting a surface.

Total solar radiation G: The sum of the beam and the diffuse radiation on a surface.

$$G_b = G_{b,n}\cos(\theta) \qquad \textit{Eq. 3}$$

$$G_{d,h} = G_h - G_{b,h} \qquad \textit{Eq. 4}$$

$$G_{b,h} = G_{b,n}\cos(\theta_z) \qquad \textit{Eq. 5}$$

G_b = the direct radiation towards a tilted surface

$G_{b,n}$ = the direct radiation towards a surface perpendicular to the sun

θ = angle of incidence for the direct radiation against the tilted surface

$G_{d,h}$ = diffuse radiation towards a horizontal surface

G_h = the total radiation towards a horizontal surface

$G_{b,h}$ = the direct radiation towards a horizontal surface

θ_z = angle of incidence for the radiation against a horizontal surface (zenith angle)

Figure 14 illustrates where *Eq. 3*, *Eq. 4* and *Eq. 5* are coming from.

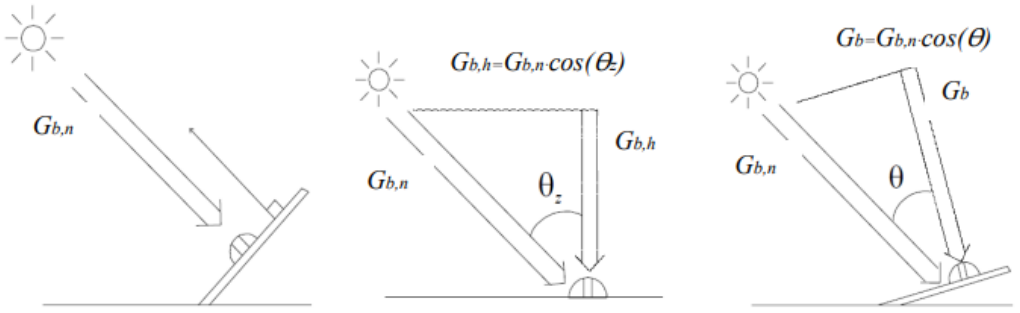

Figure 14 Graphical representation of beam, beam normal and beam horizontal radiation (Björn O Karlsson, 2022)

2.4.3.2 Calculation of diffuse radiation

Anysotropic model – Hays and Davies Model

This model splits diffuse radiation in two parts, from the angles close to the sky and from the rest of the sky.

$$G_d = \frac{Gd,h(1-Ai)(1+\cos(\beta))}{2} + \frac{Gd,h*Ai*\cos(\theta)}{\cos(\theta z)} \qquad \textit{Eq. 6}$$

$$A_i = \frac{G_{bn}}{Gon} \qquad \textit{Eq. 7}$$

$$G_{o,n} = 1367*\left(1 + 0.033\cos\left(360 * \frac{n}{365}\right)\right) \qquad \textit{Eq. 8}$$

G_d = diffuse radiation towards the tilted surface (W/m^2)

β = tilt of the surface from the horizontal (°)

$G_{o,n}$ = radiation outside the atmosphere towards a surface perpendicular to the sun (W/m^2)

A_i = anisotropic-index. Measure on the transmittance of direct radiation through the atmosphere.

n = day number of the year

Isotropic model

It is a simple model in which the diffuse radiation is assumed to have the same intensity from the entire sky. The equation is the same as using Ai = 0 in Eq. 6.

$$G_d = \frac{G_{d,h}(1+\cos(\beta))}{2} \qquad \textit{Eq. 9}$$

2.4.3.3 Calculation of ground reflected radiation

Apart from the direct, G_b, and the diffuse, G_d, radiation towards a tilted surface there is also ground reflected radiation, G_g. The ground reflected radiation is normally assumed to be isotropic.

$$G_g = \frac{\rho_g G_h (1 - \cos(\beta))}{2} \qquad \textit{Eq. 10}$$

Being ρ_g the reflectance of the ground and $(1-\cos(\beta))/2$ the surface view factor against the ground.

In the excel file of WINSUN G_d and G_g are summed to form G_{diffus}

2.4.3.4 Calculation of total radiation

Taking into consideration the results obtain with *Eq. 3*, *Eq. 9*, and *Eq. 10* the value of the total radiation can be obtained.

$$G = G_b + G_d + G_g \qquad \textit{Eq. 11}$$

(Björn O Karlsson, 2022)

2.4.4 Solar angles

2.4.4.1 Declination

The angle of declination (δ) corresponds to the angle between the line of the equator and a line that goes from the center of the Earth to the sun. It goes from +23.45° in the summer solstice to -23.45° in the winter solstice.

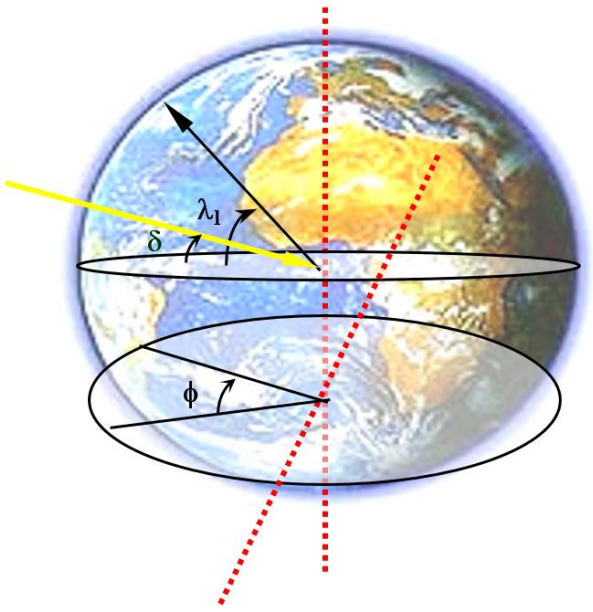

Figure 15 Representation of the declination angle δ together with the latitude λ (λ_l in figure) and longitud L

$$\delta = 23.45 \sin\left(360 \frac{284 + n}{365}\right) \qquad \textit{Eq. 12}$$

L = Longitude, the angular location west of Greenwich England $0° \leq L \leq 360°$.

λ = Latitude, the angular location north or south of the equator, north positive; $-90° \leq \lambda \leq 90°$(Björn O Karlsson, 2022).

2.4.4.2 Solar time and hour angle

Solar time is the time used in all sun-angle relationships; it does not coincide with local clock time. It is necessary to convert standard time to solar time by applying two corrections. There is a constant correction for the difference in longitude between the observer's meridian (longitude) and the meridian on which the local standard time is based. The second correction comes from the equation of time, which considers the perturbations in the Earth's rotation rate that affect the time the Sun crosses the observer's meridian.

$$\text{Solar time} - \text{standard time} = 4(L_s - L_l) + E \qquad \textit{Eq. 13}$$

L_s = standard meridian for the local time zone

L_l = longitude of the location, $0^o < L_l < 360^o$

$$E = 229.2(0.000075 + 0.001868\cos B - 0.032077\sin B - 0.014615\cos 2B - 0.04089\sin B) \qquad \textit{Eq. 14}$$

$$B = \frac{360(n-1)}{365} \qquad \textit{Eq. 15}$$

The hour angle is the angular displacement of the sun, it can be in the direction of the east or west of the local meridian due to rotation of the earth on its axis at 15° per hour with morning being negative and afternoon being positive.

$$\omega = 15 * (hh - 12) + \frac{mm + E}{4} + (L_s - L_l) \qquad \textit{Eq. 16}$$

ω = hour angle

hh = hours

mm = minutes (Björn O Karlsson, 2022)

2.4.4.3 Angles for solar panel position

$\beta =$ Tilt, the angle between the plane of the surface in question and the horizontal; $0\circ \leq \beta \leq 180\circ$. ($\beta > 90\circ$ means that the surface has a downward-facing component.)

$\gamma =$ Surface azimuth angle, the deviation of the projection on a horizontal plane of the normal to the surface from the local meridian, with zero due south, east negative, and west positive; $-180\circ \leq \gamma \leq 180\circ$.

$\theta =$ Angle of incidence, corresponds to the angle between the beam radiation on a surface and the normal direction to that surface (Duffie et al., 2020).

$$\theta = \arccos(\cos(\delta)\sin(\omega)\sin(\beta)\sin(\gamma) + \cos(\delta)\cos(\omega)\sin(\lambda)\sin(\beta)\cos(\gamma) - \sin(\delta)\cos(\lambda)\sin(\beta)\cos(\gamma) + \cos(\delta)\cos(\omega)\cos(\lambda)\cos(\beta) + \sin(\delta)\sin(\lambda)\cos(\beta)) \quad \textit{Eq. 17}$$

2.4.4.4 Angles for the position of the sun in the sky

θz = Zenith angle, the angle between the vertical and the line to the sun, that is, the angle of incidence of beam radiation on a horizontal surface. For the calculation of the zenith angle the equation is the same one as Eq. 17 but with $\beta = 0$, as it is the angle of incidence for horizontal surfaces.

$$\theta = \arccos(\cos(\delta)\cos(\omega)\cos(\lambda) + \sin(\delta)\sin(\lambda)) \quad \textit{Eq. 18}$$

αs = Solar altitude angle, the angle between the horizontal and the line to the sun, that is, the complement of the zenith angle (Duffie et al., 2020).

$$\alpha_s = \arcsin(\cos(\delta)\cos(\omega)\cos(\lambda) + \sin(\delta)\sin(\lambda)) \quad \textit{Eq. 19}$$

γs = Solar azimuth angle, corresponds to the angular displacement from south of the projection of beam radiation of the sun on the horizontal plane. Displacements east of south are negative and west of south are positive (Björn O Karlsson, 2022).

$$\gamma_s = \arcsin\left(\frac{\cos(\delta)\sin(\omega)}{\cos(\alpha_s)}\right) \quad \textit{Eq. 20}$$

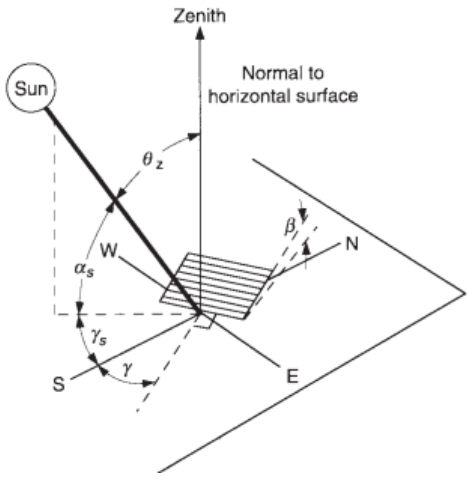

Figure 16 Description of the zenith angle, surface azimuth angle, solar azimuth angle for a tilted surface, and tilt (Duffie et al., 2020.)

2.5 WINSUN Equations

The WINSUN software has been used for the development of this work. This is a simplified program developed in HiG that is able to show the photovoltaic energy production in a year by entering hourly data of temperature, horizontal diffuse irradiance, global horizontal solar irradiance and characteristics of the PV-installation. In addition, other values representative of the location of the solar installation must be entered.

2.5.1 Calculation of the performance of a PV-system in WINSUN

For the calculation of the power output for each of the timesteps, the equation used will be the following.

$$P(T,\theta) = \frac{P(25,0) * (Kb(\theta) * Gb + Kd * Gd)(1 + (Tcell - 25) * \alpha)}{1000} \qquad \textit{Eq. 21}$$

On the other hand, the calculation of the efficiency will be done with:

$$\eta(T,\theta) = \frac{P(T,\theta)}{A_{PVsystem}} \qquad \textit{Eq. 22}$$

P(25,0) = Power at STC (Standard Test Conditions)

The STC consists of the conditions in which the output power of the solar panels is measured.

With a solar irradiance of 1000 W/m2, Tcell of 25ºC and AM (Air mass) of 1.5.

K_d = Correction factor for diffuse irradiation, Kd =0,925 will be used

$K_b = 1-(\tan(\theta/2))^p$ Correction factor for direct irradiation

p = angular dependent coefficient, value introduced p = 4

α = coefficient for temperature dependence of PV-module ≈ -0,4%/ C for crystalline Silicon, value introduced $\alpha = 0.004$

$A_{PV\text{-}SYSTEM}$ = Area of the solar panels of the PV-system (Karlsson, 2022)

2.5.1.1 Calculation of the angle of incidence towards module and horizontal

For the calculation of incidence θ Eq.17 and solar altitude αs Eq. 19 some previous calculations have been done. Calculations for solar time, hour angle ω, and declination δ using Eq. 12 – Eq.16 .

2.5.1.2 Calculation of the irradiation on the modules

Eq. 3 is used for the calculation of direct or beam radiation G_b on modules taken into consideration the input data received, diffuse horizontal radiation $G_{d,h}$ and global horizontal radiation G_h. Eq. 6 is used for the calculation of the diffuse radiation G_d on modules what means that the anisotropic model has been chosen. Eq. 10 is used for the calculation of the ground radiation on modules G_g. And Eq. 11 is used for the total radiation G.

2.5.1.3 Estimation of the temperature of the module

The temperature of the module is estimated by the program using the following equation.

$$T_{cell} = T_{ambient} + G * \frac{n_0 - \eta}{h} \qquad \textit{Eq. 23}$$

η = Efficiency of modules

h = Heat transfer coefficient for heat losses between modules and ambient, value introduced h = 20 W/(m^2*K)

n_0 = thermal solar absorption of the PV modules

(Karlsson, 2022)

3 Method

This project is a case study that will be carried out at the University of Gävle, specifically in building 45 (60° 40' 3.558" N , 17° 6' 47.6028" E), were different types of photovoltaic solar panels are located. Among these, the study will be realized on the Eoplly 190 Watt Solar Panel of monocrystalline type tilted 45º and with an azimuth solar angle of 0º (e.g., facing south). The data available of the electricity generation consists of data from April 2021 to February 2024 and three different files have been provided, in which data is recorded every minute, every 10 minutes and every day. In addition to the electricity production, these files also contain the radiation data obtained from the three pyranometers located just 15 meters away from the photovoltaic panels. These pyranometers measure the horizontal global radiation, diffuse horizontal radiation, and one of them is tilted 45º and with an azimuth angle of -12.5º measuring the global radiation. Radiation data will be changed to hourly data and together with temperature data they will be introduced in the WINSUN software based on Microsoft Excel to compare the measured data with the pyranometers with the electricity produced. Other types of studies could have been performed, but the most convenient is the one chosen because in this way we can better reach the conclusions we are seeking of making an accurate and reliable climate file for the city of Gävle.

3.1 PV installation

3.1.1 Location

The place where this case study has been carried out is the building 45 of the University of Gävle, a city in the center of Sweden. The exact coordinates of the building's location are (60° 40' 3.558" N, 17° 6' 47.6028" E) in degrees, (60.67 N, 17.11 E) in decimal. Located in Sweden, Gävle has a climate with four distinct seasons. Winters bring frigid temperatures averaging around freezing and frequent snowfall. Summers provide mild temperatures. Precipitation is a constant throughout the year, with rain more common during the warmer months and snowfall in winter months. Overall, Gävle offers a clear contrast between cold, snowy winters and milder, wetter summers.

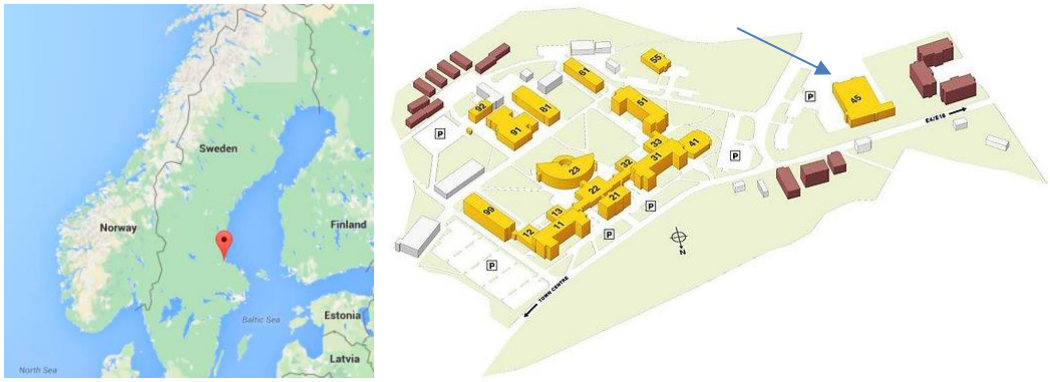

Figure 17 Location of the study

Figure 17 shows the exact location of the study, the one of the city of Gävle and the one of the building 45 in the university.

3.1.2 Solar panels

The solar panels used in this study are the Eoplly 125M/ 72 (195 W), some monocrystalline solar panels, whose data sheet can be seen in Appendix A. The PV-system located in building 45 consists of 6 solar panels giving a total of 1.17 kWp, which are oriented perfectly to the south, with an azimuth angle γ of 0º and tilted β 45º.

Figure 18 PV-system of building 45 in the university of Gävle

3.1.3 Inverter

The inverter used in the PV-system in charge of changing from DC to AC is one of the brand SMA Solar Technology and the model is SUNNY BOY 1200. The data sheet for this inverter can be found in Appendix A.

Figure 19 SUNNY BOY 1200 inverter(Solar Technology, n.d.)

3.1.4 Pyranometers

A pyranometer is an instrument for measuring the total hemispheric solar radiation or global radiation (direct plus diffuse radiation), usually on a horizontal surface. (Duffie et al., 2020.)

Next to the PV-system studied, three different pyranometer are located, giving each of these ones different values. Figure 20 shows two different pyranometers, the one placed on the left (*pyranometer 2*) is in charge of measuring the total radiation towards a horizontal surface G_h. The one on the right (*pyranometer 1*) measures the total radiation towards a tilted surface, with a tilt of $\beta = 45^o$ and an azimuth angle of γ = -12.5° (12.5° to the East) which corresponds to the direction of the building.

Figure 20 Pyranometers in building 45 measuring total radiation in a horizontal surface and in a tilted surface

When shaded from direct radiation by a shading ring or disk, a pyranometer measures diffuse radiation. Which exactly are the measurements that the third pyranometer (*pyranometer 3*) takes (Figure 21). The pyranometer is shaded from the beam radiation and it allows the recording of diffuse radiation without the necessity of continuous positioning of smaller devices (Duffie et al., 2020.). The position of the shaded ring is to be changed weekly in order to get accurate data of the diffuse radiation. As the ring shades from part of the diffuse radiation a correction factor should be introduced, oscillating from 1.05 to 1.2 (Drummond, 1956). In this study this correction factor will be neglected because it will not affect the results in a major way. The data obtained with this pyranometer is the diffuse radiation towards a horizontal surface $G_{d,h}$.

Figure 21 Pyranometer with a shading ring taking diffuse radiation

Measurements obtained with the pyranometers have been later introduced in the WINSUN program.

3.2 Data collection

3.2.1 Data logger

The data logger responsible for recollecting all the data from the PV-system and the pyranometers is the Data logger Cambell Scientific CR 1000 (Figure 22). This logger will give the data of the energy output of the PV-system in kWh, and data from the three pyranometers measuring $G_{d,h}$, G_h and $G_{45°,-12.5°}$ (tilted surface). The logger provides data for different time intervals, for every minute, for every ten minutes and for every day. In this work we will use the file that collects data per minute to transform it into hourly data and thus be able to enter them into the WINSUN program.

*Figure 22 Data logger Campbell Scientific CR 1000 (*CR1000: Measurement and Control Datalogger*, 2007.)*

3.3 Climatic data

3.3.1 Temperature data

Temperature data from building 45 was provided, but due to the lack of data in a lot of different hours, it was decided to look for an alternative. This alternative consisted in taking temperature values from the Swedish Meteorological and Hydrological Institute (SMHI) website which provides hourly values. In the absence of certain temperature values again in this file, it was decided to make a linear approximation, giving the average temperature value between the previous and following hour in the hours when no data was available. Figure 23 gives a perspective of the distance between the SMHI meteorological station (Gävle A) and the university of Gävle where the photovoltaic installation under study is located.

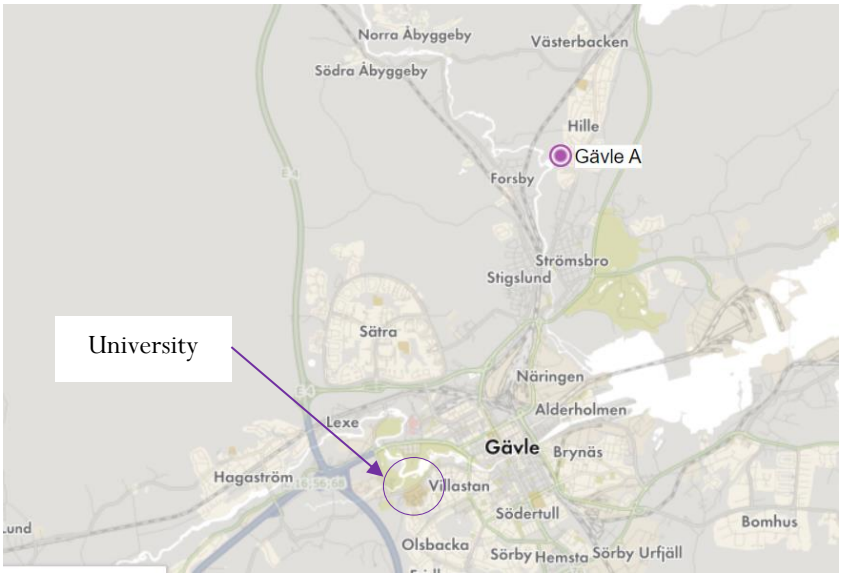

*Figure 23 Location where temperature data was collected (*Ladda Ner Meteorologiska Observationer | SMHI*, n.d.)*

3.3.2 Snow data

Snow data has also been taken from the same website SMHI and same location (Gävle A). The collected data is given in meters as daily data and will give the possibility of comparing PV production with snowfall.

3.4 WINSUN program

As has been stated before, the WINSUN program is a Microsoft Excel based program developed in the University of Gävle in 2001. The program is based on many years of long-term measurements and efficient modeling of both solar radiation, solar thermal and photovoltaic yields dating back to the 1970s. WINSUN PV has been based on a version used and validated from 2001 at the Technical University of Denmark (DTU) in Copenhagen for estimating the energy yield from large solar thermal systems to district heating.

Instead of using the WINSUN website the software will be used directly, to enable more precise results. Some input data must be introduced, detailing the characteristics of the location and of the PV-system as well as some climate data, such as, hourly data of temperature, horizontal diffuse irradiance and global horizontal solar irradiance. After introducing the input data, the energy output for each of the months of the year is obtained.

The calculation model for solar production was developed by Björn O Karlsson and Bengt Perers from the University of Gävle.

3.4.1 Input data

Table 1 shows some of the input data that has been introduced, the PV-system illustrated in Figure 18 has the values of β and γ represented in the table. ρ_g has taken the value 0.1 because asphalt is the material of the ground that surrounds the installation. The most typical value for the horizontal shading has been selected.

Table 1 PV input data for the studied localization

PV local input data	**Value**	**Unit**
Tilt (β)	45	º
Direction, azimuth (γ)	0	º
Ground reflection (ρ_g)	0.1	º
Horizontal shading	10	º

Table 2 displays the values of the maximum peak power of the 6 solar panels, each of them has 195 Wp. Each of the solar panels' area is 1 m^2. And the system efficiency displayed corresponds to the electrical system efficiency including inverter MPP tracking and DC/AC conversion plus losses in cables and any module MPP electronics etc.

Table 2 Characteristics of the PV modules

PV system input	**Value**	**Unit**
Pmpp	1.17	kWp
Area of modules	6	m^2
System efficiency	0.912	-

Other interesting values that have been entered are the values of latitude and longitude of the PV- installation, which have been shown in 3.1.1. On the other hand, values from modules encapsulate other input data that has been entered into the program taking the most common possible values (Table 3).

Table 3 Detail input data for the PV modules

Detail input data	**Value**	**Unit**
no thermal solar absorption	0.9	-
h heat loss coefficient	20	W/(m^{2}K)
p angle-dependent coefficient of direct sunlight	4	-
Kd diffuse acceptance coefficient	0.925	-
Coefficient for temperature dependence	0.004	1/K

3.5 Diffuse radiation towards a horizontal surface $G_{d,h}$

3.5.1 Processing of data entered into WINSUN in 2023

The first data analysis was carried out for the year 2023. One of the problems identified in the study was the inaccuracy of measurements of diffuse radiation towards a horizontal surface. Figure 24 depicts both $G_{d,h}$ and G_h during the year 2023, four zones within the graph are the most striking ones. In these zones the diffuse horizontal radiation takes similar values to the global horizontal radiation, what means that in the dates this has happened the shading ring of *pyranometer 3* has not been correctly placed. The shading ring as stated in 3.1.4 should prevent direct radiation from directly impacting the pyranometer, so that it only captures the diffuse radiation when in shadow. Nevertheless, as the shading ring has not been correctly placed, the values of the horizontal diffuse radiation and the horizontal global radiation coincide in the rounded areas, the *pyranometer 3* in those moments has registered values higher than those that should correspond to it. Data from *pyranometer 3* should be adjusted.

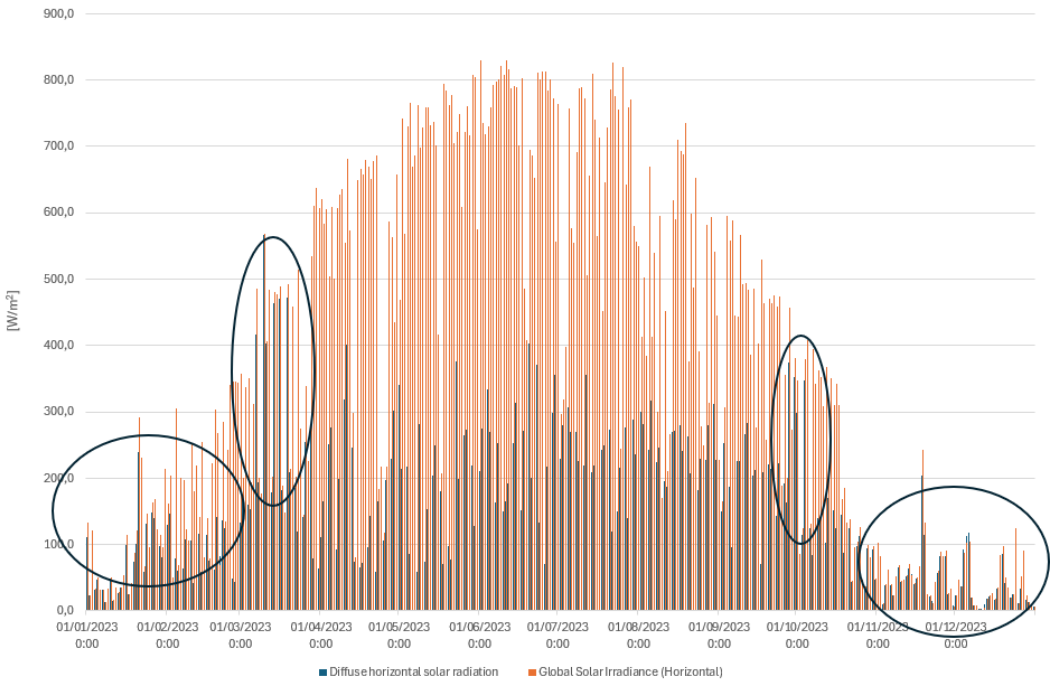

Figure 24 Comparison between the $G_{d,h}$ and the G_h in 2023 in HiG (Measurements taken by the pyranometers 2 and 3)

In order to adjust the value of the $G_{d,h}$, a series of calculations have been developed. The equations that have been used for the calculations have been previously explained in section 2.4.3.1–2.4.3.4. Eq. 24 shows the formula to obtain $G_{d,h}$ dependent on different parameters. Due to the small expected value for ground reflected radiation G_g it has been decided to neglect this term.

$$Gd,h = \frac{G - G_h * R}{\left(\frac{1+\cos(\beta)}{2}\right) - R} \qquad \textit{Eq. 24}$$

$$R = \frac{\cos(\theta)}{\cos(\theta_z)} \qquad \textit{Eq. 25}$$

R = Geometry factor

In Eq. 24 data collected from *pyranometer 1* has been introduced as G, being the solar global radiation measured at $\beta = 45°$ and $\gamma = -12.5°$, and data collected from *pyranometer 2* has been introduced as G_h. Once the results were obtained, certain errors in the summer months were appreciated since in these months the value of the denominator of Eq. 24 picked up values close to 0 which made the values for $G_{d,h}$ shoot up (Figure 25). This led to the need to apply further adjustments to the horizontal diffuse radiation values. What is interesting is that for the areas where Figure 24 showed errors due to shading ring misplacement, Eq.24 projects more accurate $G_{d,h}$ values.

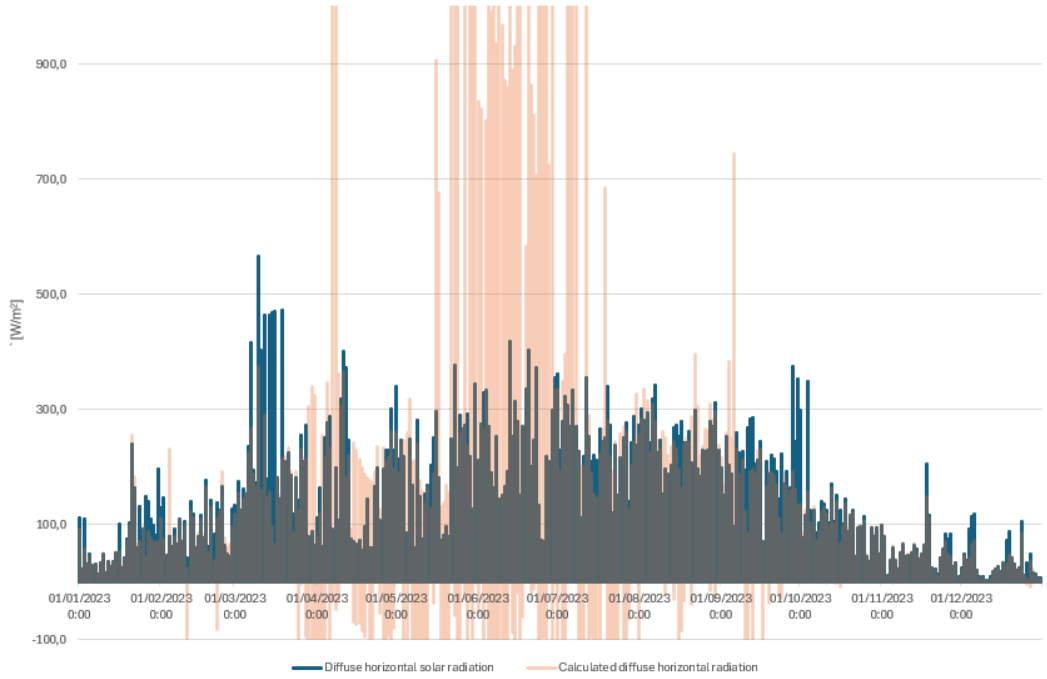

Figure 25 Comparison between measured diffuse horizontal radiation and calculated one with Eq. 24 in 2023

After observing the errors in Figure 25, the next adjustment consisted of comparing both calculated and measured values and determining as valid the one with values less than half of the global horizontal radiation G_h. In the case that neither of the two values was less than half of the global horizontal radiation G_h or the calculated values of $G_{d,h}$ were negative, the measured values were chosen as the default values.

$$F_d = \frac{G_d}{G} \qquad \textit{Eq. 26}$$

The diffuse fraction F_d was decided to be limited as 0.5 in the adjustments showed above, due to a study carried out by (Jamil & Akhtar, 2017)in which they were testing different models for the estimation of the G_d and they obtained average values for the three years studied of $F_d = 0.37$.

Figure 26 illustrates how the shape of the diffuse horizontal radiation profile changed after the adjustments were made. The main peaks that could be seen in the months of March and October have been reduced. These could have caused major alterations in the desired results of PV energy obtained.

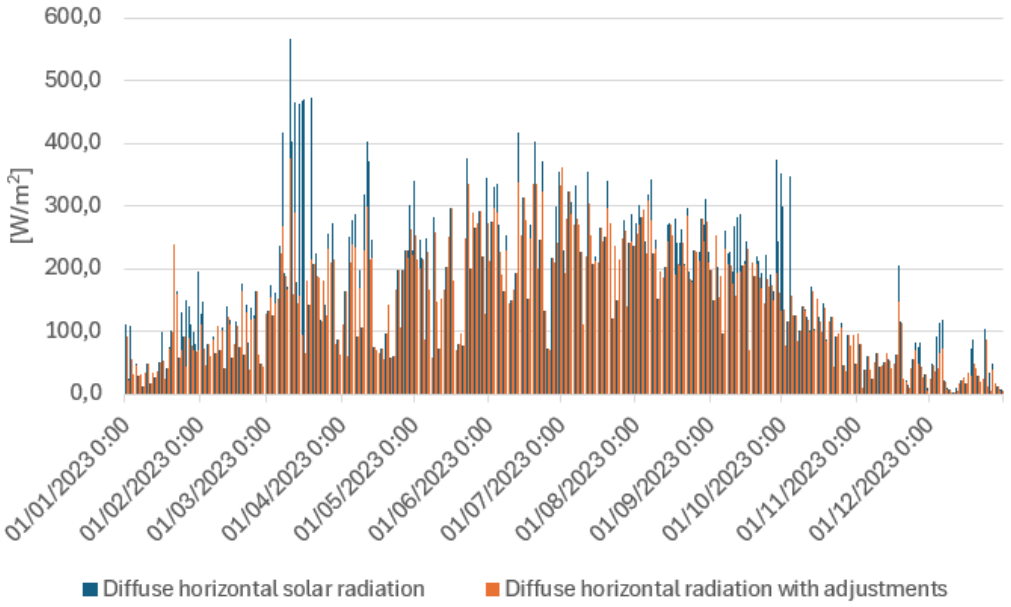

Figure 26 Comparison of the measured diffuse horizontal radiation and the adjusted one in 2023

Figure 27 illustrates both global horizontal radiation G_h and adjusted diffuse horizontal radiation $G_{d,h}$. As explained above, the errors due to the poor positioning of the shading ring in March and October have been corrected and can be seen by comparing Figure 24 with Figure 27. However, looking at Figure 27 it can be seen that certain peaks existing at certain times, these will be disregarded due to the little influence they will have on the results. During the winter period, similar values are still seen between the horizontal diffuse radiation $G_{d,h}$ and the horizontal global radiation G_h. Since it has little influence on the results, the input data $G_{d,h}$ entered in WINSUN will remain as they are.

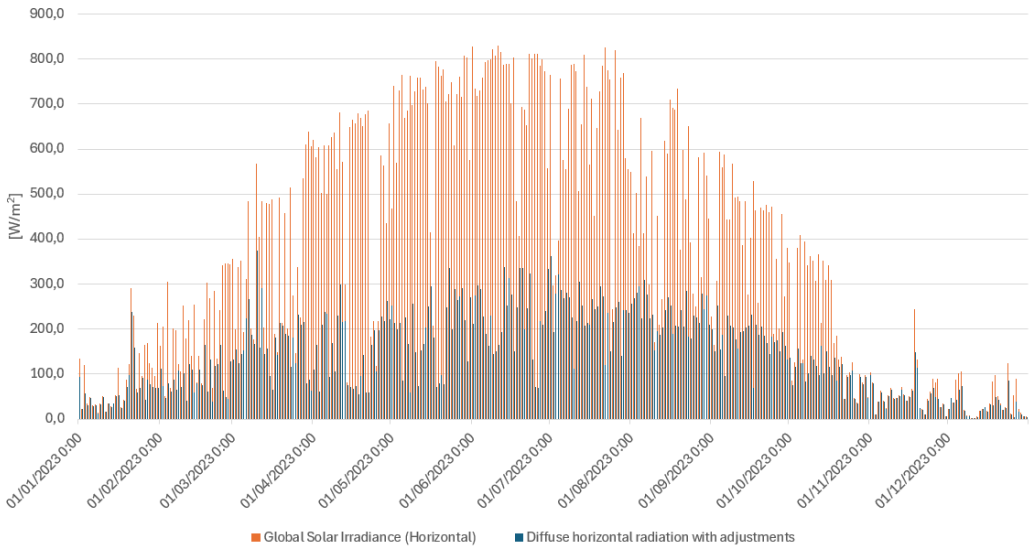

Figure 27 Comparison of the global horizontal radiation with the adjusted diffuse horizontal radiation in 2023

Figure 28 and Figure 29 illustrate monthly data of global, diffuse, and direct horizontal radiation for the year 2023. Figure 28 shows monthly data where it can be seen how in the last months of the year and mainly in March, due to the poor adjustment of the shadowing ring, the diffuse radiation exceeds the direct or beam radiation. This problem is solved as can be observed in Figure 29.

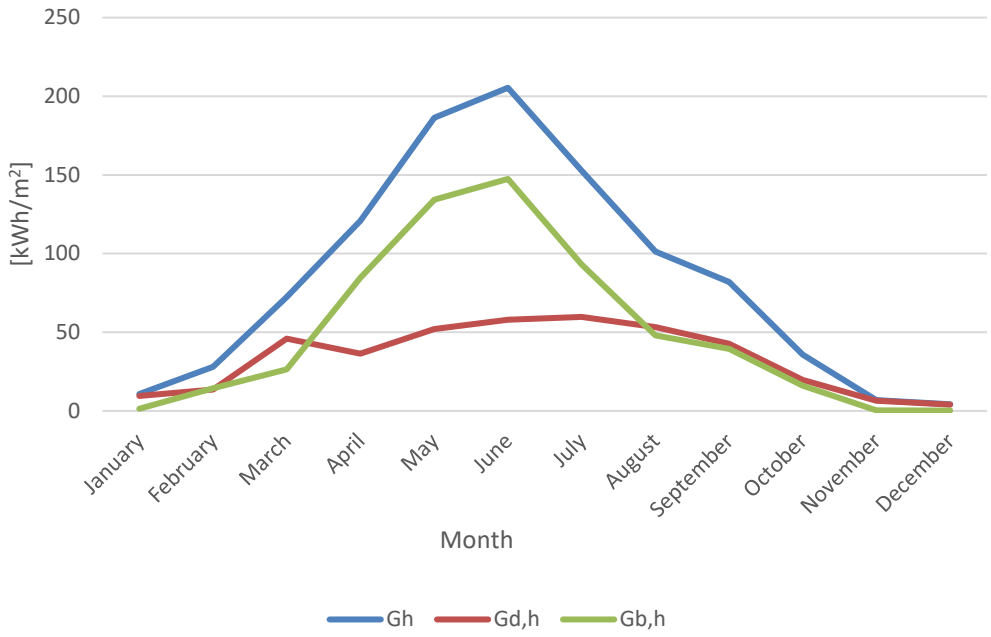

Figure 28 Monthly data for G_h, $G_{d,h}$, $G_{b,h}$ with raw data 2023

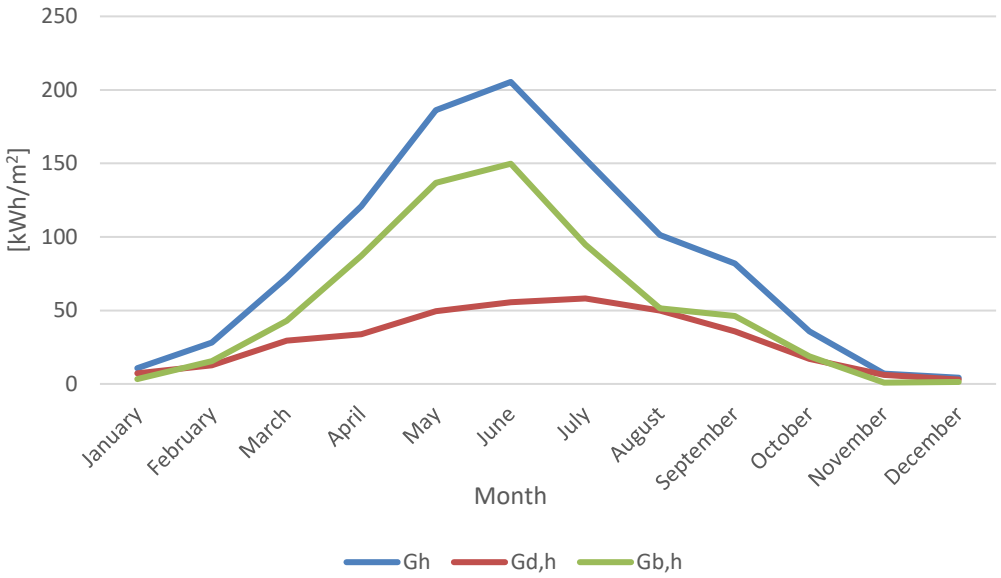

Figure 29 Monthly data for G_h, $G_{d,h}$, $G_{b,h}$ with adjusted data 2023

3.5.2 Processing of data entered into WINSUN in 2022

Data for the year 2022 was processed in the same way as it was done with the data corresponding to 2023. Similar to Figure 24, Figure 30 presents time lapses (rounded zones) in which the shading ring has not been correctly placed and the horizontal diffuse radiation values are similar to those of the global horizontal radiation. Therefore, it was proceeded to perform the same calculations as for the year 2023.

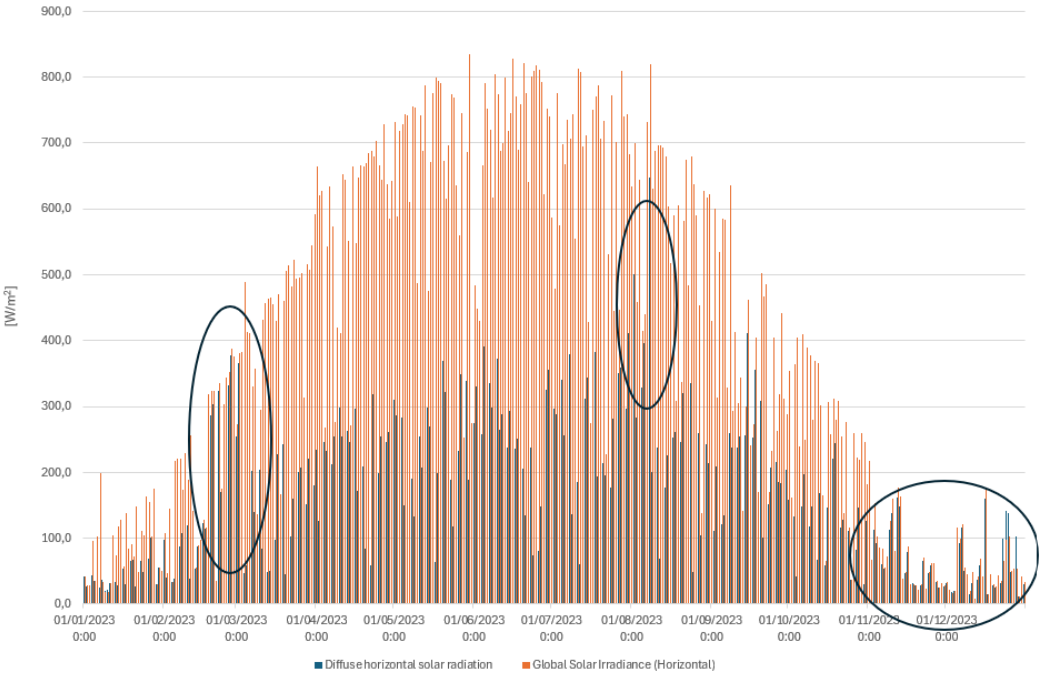

Figure 30 Comparison between the $G_{d,h}$ and the G_h in 2022 in the HiG (Measurements taken by the pyranometers 2 and 3)

After making calculations with Eq. 24 the results obtained were the ones presented in Figure 29.

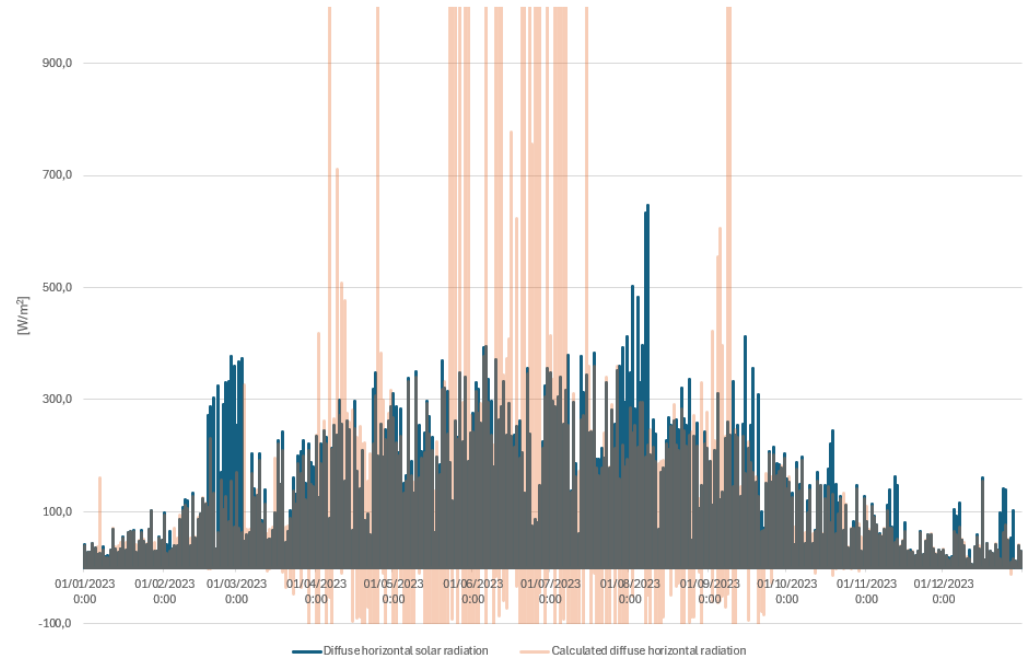

Figure 31 Comparison between measured diffuse horizontal radiation and calculated one with Eq. 24 in 2022

Using the values of both series new values were obtained for $G_{d,h}$ with the same adjustments done in 2023 data. Figure 32 illustrates how the profile of the adjusted diffuse radiation does not have the peaks of the end of February and beginning of August.

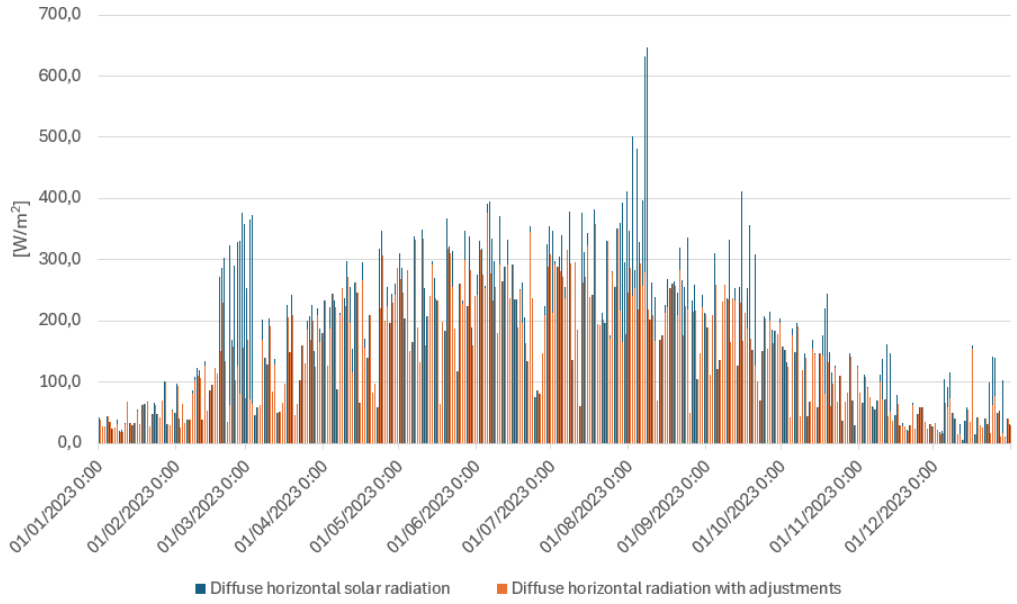

Figure 32 Comparison of the measured diffuse horizontal radiation and the adjusted one in 2022

Figure 33 depicts both global horizontal radiation G_h and adjusted diffuse horizontal radiation $G_{d,h}$. Less peaks than in Figure 27 can be observed, which apparently could lead one to believe that the results obtained for the year 2022 will be more accurate.

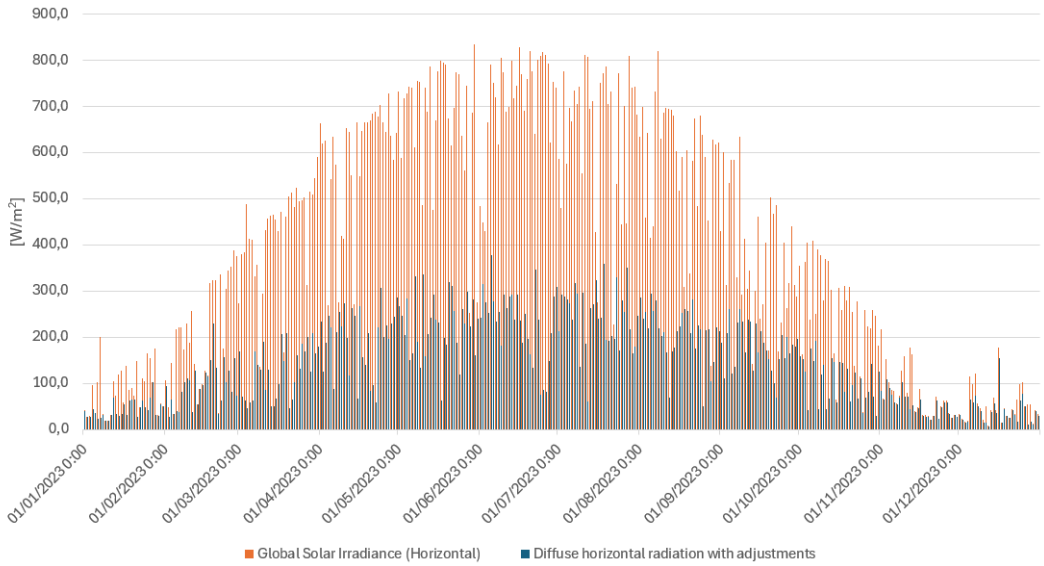

Figure 33 Comparison of the global horizontal radiation with the adjusted diffuse horizontal radiation in 2022

As it can be observed in Figure 34 and in a similar way as it has happened in 2023, there are certain months in which the $G_{d,h}$ is higher than the $G_{b,h.}$ Figure 35 illustrates how this values of $G_{d,h}$ have been adjusted.

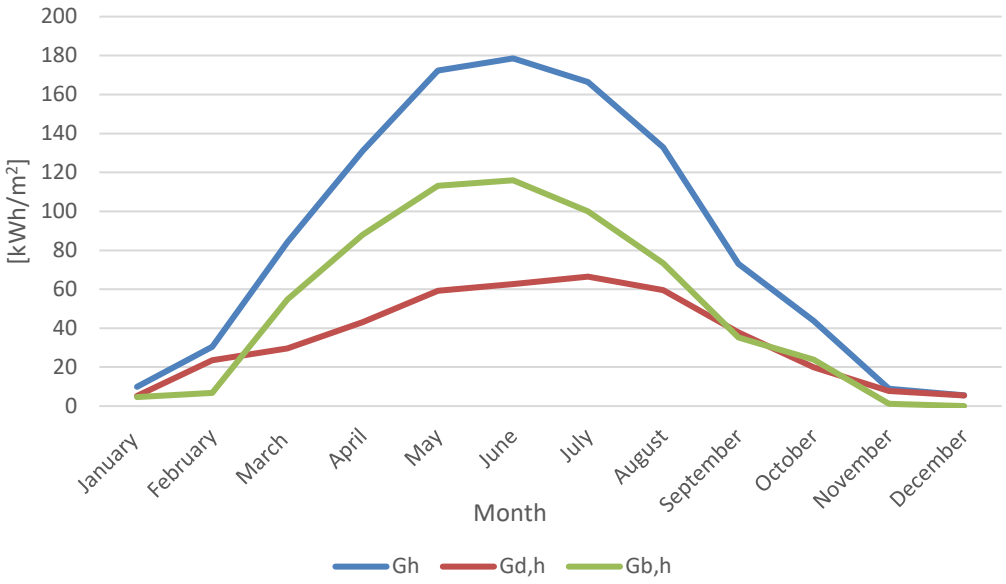

Figure 34 Monthly data for G_h, $G_{d,h}$, $G_{b,h}$ with raw data 2022

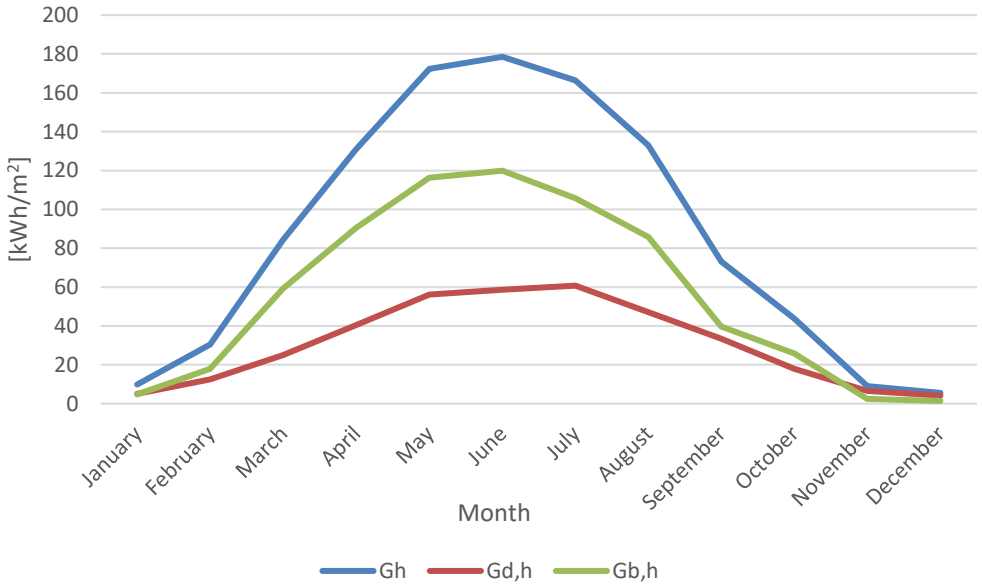

Figure 35 Monthly data for G_h, $G_{d,h}$, $G_{b,h}$ with adjusted data 2022

3.6 Comparison between $G_{45º/-12.5º}$ measured and simulated

In order to be able to determine the PV output, it must be checked whether the input values after adjustment result in accurate values. Therefore, it has been decided to compare the radiation data at $\beta = 45°$ and $\gamma = -12.5°$ detected with the *pyranometer 1* with the radiation data obtained with the WINSUN program with the parameters established in section 3.4.1. Figure 36 and Figure 37 perfectly show the correlation between both data, despite the months of January and December. This could be due to the value introduced for the horizontal shading because it neglects the radiation when αs is lower than it.

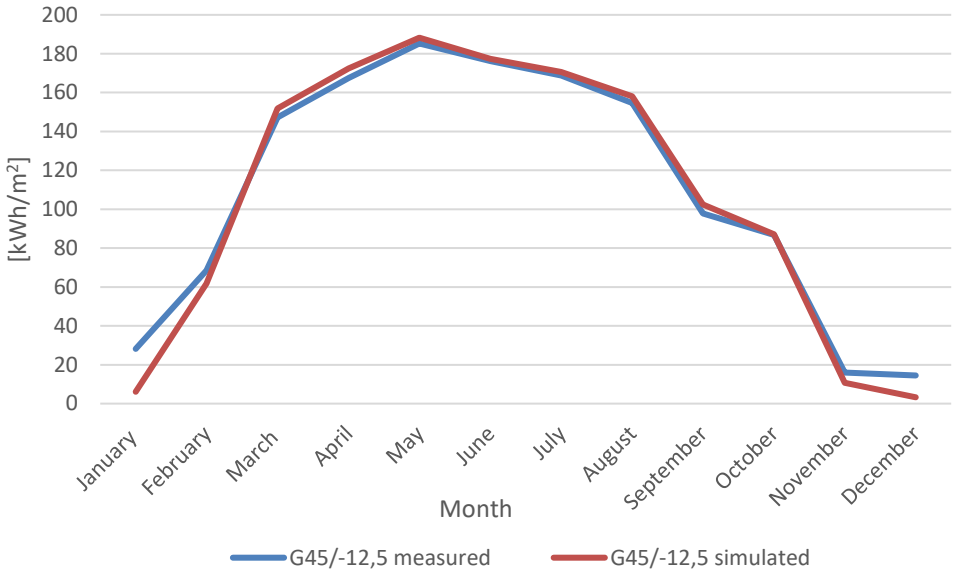

Figure 36 Comparison between $G_{45°/-12.5°}$ measured and simulated in 2022

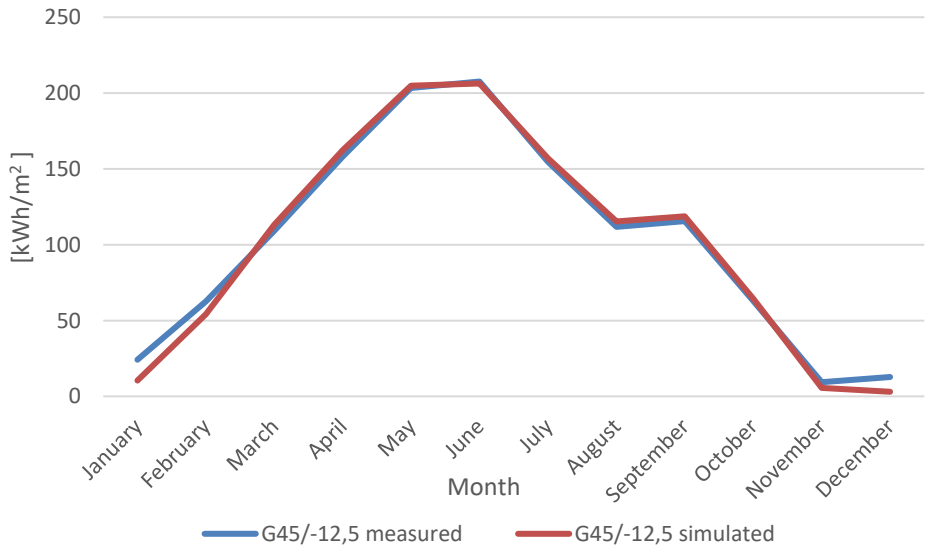

Figure 37 Comparison between $G_{45°/-12.5°}$ measured and simulated in 2023

Figure 38 illustrates the months in which disparities between measured and simulated data are higher. With 78% less radiation in simulated data in both January and December in 2022.

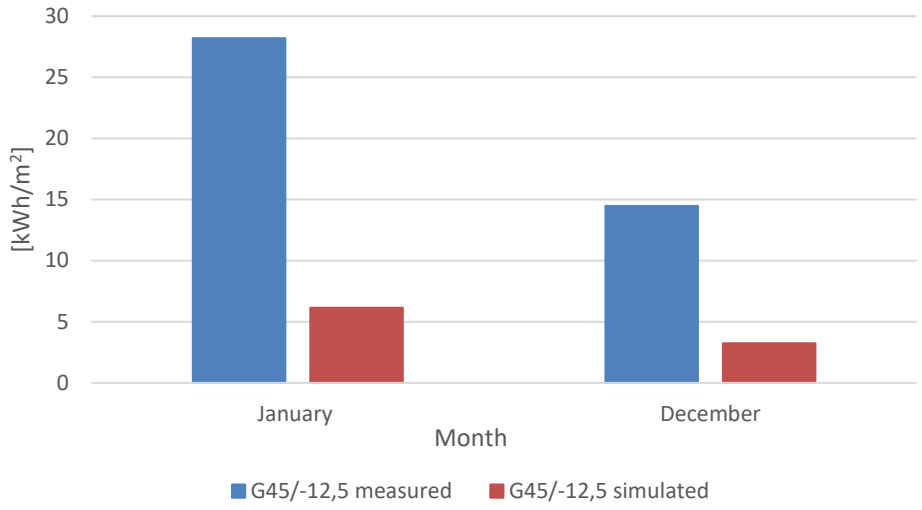

Figure 38 Difference between $G_{45°/-12.5°}$ measured and simulated in January and December 2022

Figure 39 shows that simulated data is 57% less in January and 76% less in December with respect to the measured values.

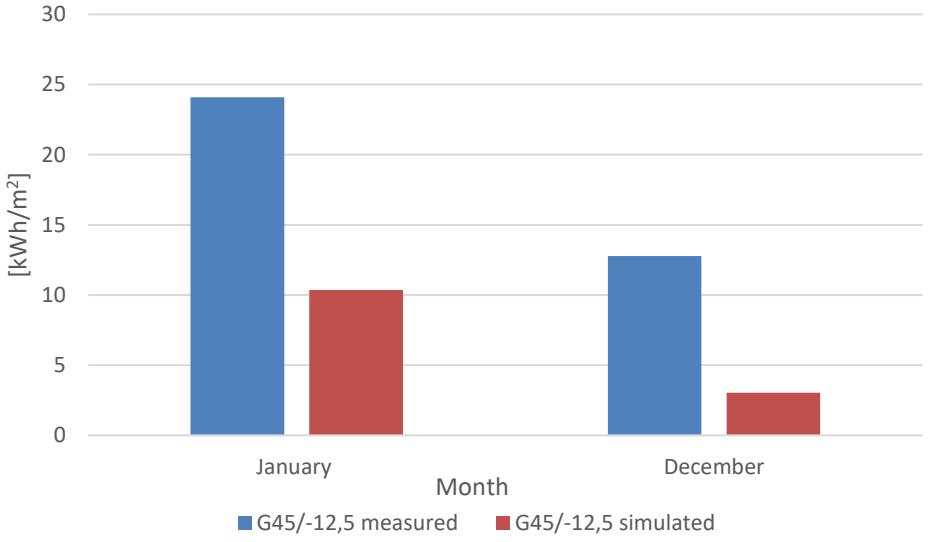

Figure 39 Difference between G45°/-12.5° measured and simulated in January and December 2023

3.7 Statistical comparison

The results obtained with the method shown above will be evaluated and compared using different statistical methods. There are different studies in which experimental values are compared with values obtained by different models created such as (Torres et al., 2010), in which statistical methods for the determination of errors are used, Mean Bias Difference (MBD) and Root Mean Square Difference (RMSD).

After doing some research, it has been seen that due to the lack of precision of the error evaluation of these methods, other studies have decided to use different statistical methods (Gueymard, 2014). With this in mind, (Behar et al., 2015; Despotovic et al., 2015; Jamil & Akhtar, 2017)decided to introduce the global performance indicator (GPI) which is a combination of five statistical methods. The equations that have been used for the determination of the GPI can be found in Appendix B.

3.8 Other sources for PV output

In order to validate the results obtained above and to confirm their accuracy, different data sources and web pages for the calculation of the PV output will be used.

3.8.1 Photovoltaic Geographical Information System (PVGIS)

PVGIS is one of the sources that will be used, which is a website that is able to give information about a PV-system performance in almost any place in the world. This website calculates the radiation of the place where the study is being carried out with satellite images, which mainly evaluate the influence the effects of the clouds in the radiation received and it is said to have a resolution of 30 km (*PVGIS Data Sources & Calculation Methods - European Commission*, 2020.).

To obtain the results of the PV output with PVGIS the database used was PVGIS-SARAH2, whose data has been validated with several ground stations. Crystalline silicon panels were selected as PV technology with 1.17 kWp, 16% of system efficiency, free-standing mounting position, $\beta = 45^{\circ}$ and $\gamma = 0^{\circ}$ (*JRC Photovoltaic Geographical Information System (PVGIS) - European Commission*, 2022.).

3.8.2 STRÅNG data entered into WINSUN program

The other database with which the data is to be compared is STRÅNG database. STRÅNG data is obtained by producing instantaneous fields of global radiation, UV radiation and direct radiation with a resolution of 2.5 x 2.5 km and a temporal resolution of one hour. This model covers the Nordic countries (*STRÅNG*, 2006.). STRÅNG data will then be entered into the same WINSUN program used to extract the PV output with the radiation values collected with the pyranometers.

3.8.3 WINSUN website

The latest PV output data with which comparisons will be made are the results obtained from the WINSUN website. The software of this website is the same one as the one used in this thesis. However, the results will be different from those used in this thesis because from this website the location and radiation data are less accurate. This PV output calculator uses twelve SMHI weather stations as databases and depending on the entered postal code the program will select the closest weather station. The climate file used for Gävle in WINSUN is Borlänge, which is situated 110 km to the west of Gävle with a global horizontal irradiation of 957 (kWh/m^2,year). Apart from the postal code (801 76), other data will be introduced, $\beta = 45^{\circ}$ and $\gamma = 0^{\circ}$, albedo = 0.25, horizontal shading = 10°, $P_{MP} = 1.17$ kWp and $A_{PV\text{-}SYSTEM} = 6$ m^2.

4 Results

4.1 Comparison of results with different data sources and solar production calculations softwares

4.1.1 Measured and simulated PV output comparison

Once the necessary data was obtained and entered into the WINSUN program, the PV output was extracted with the program in order to compare the results with the PV output data collected with the datalogger with the objective of validating the diffuse radiation adjustment method. In both Figure 40 and Figure 41 both measured and simulation data are compared. The results look extraordinarily accurate.

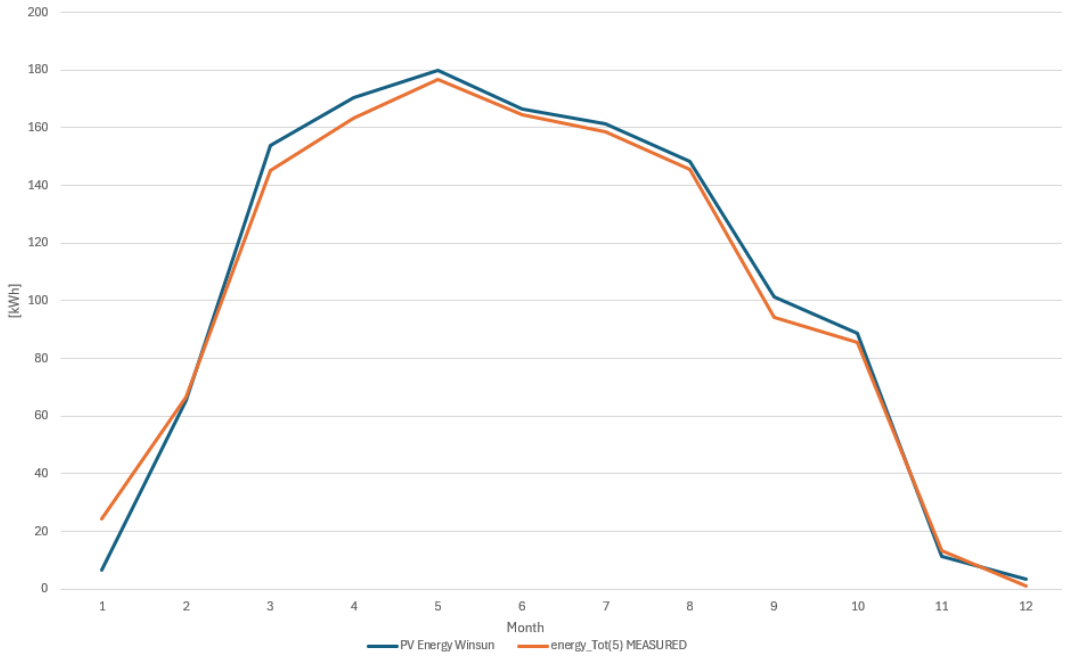

Figure 40 PV output comparison between 1.17 kW PV-system output and the simulation with WINSUN entering radiation data collected in Building 45 for 2022

In order to show the numerical difference between the data Table 4 and Table 5 are depicted.

Table 4 PV output comparison between 1.17 kW PV-system output and the simulation with WINSUN entering radiation data collected in Building 45 for 2022

Month	January	February	March	April	May	June	July	August	September	October	November	December	Total
energy_Tot(5) [kWh]	24.4	66.4	145.3	163.1	176.8	164.4	158.7	145.4	94.3	85.6	13.1	1.3	**1238.8**
PV Energy Winsun [kWh]	6.6	65.3	153.8	170.4	179.9	166.5	161.3	148.4	101.4	88.6	11.2	3.6	**1257.0**
%diff	**72.90**	**1.73**	**5.85**	**4.44**	**1.73**	**1.26**	**1.69**	**2.04**	**7.58**	**3.59**	**14.55**	**186.65**	**1.47**

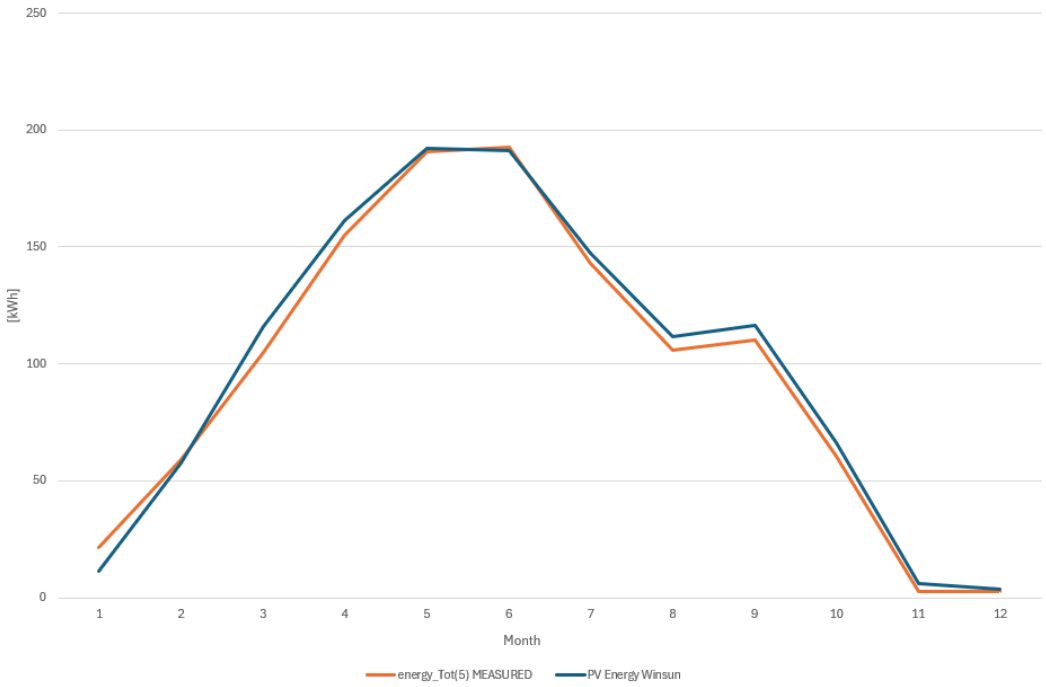

Figure 41 PV output comparison between 1.17 kW PV-system output and the simulation with WINSUN entering radiation data collected in Building 45 for 2023

Table 5 PV output comparison between 1.17 kW PV-system output and the simulation with WINSUN entering radiation data collected in Building 45 for 2023

Month	January	February	March	April	May	June	July	August	September	October	November	December	Total
energy_Tot(5) [kWh]	21.7	59.0	105.0	155.1	190.6	192.5	143.0	105.6	110.1	60.3	2.6	2.8	**1148.4**
PV Energy Winsun [kWh]	11.2	57.7	116.1	161.4	192.2	191.2	147.4	111.8	116.4	66.4	6.1	3.4	**1181.2**
%diff	**48.58**	**2.15**	**10.62**	**4.04**	**0.81**	**0.68**	**3.02**	**5.86**	**5.68**	**10.02**	**132.95**	**21.78**	**2.85**

Although the results in both years show a high similarity in the shape of the curve, in both cases the PV energy output is slightly higher in almost all months. This means that some of the input parameters entered into WINSUN need to be adjusted to increase accuracy. These parameters can be found in section 3.4.1.23

Before adjusting the parameters, some comparisons will be made with data extracted from the sources shown in 3.8.

4.1.2 Comparison with results obtained with PVGIS

Figures shown below (Figure 42 and Figure 43), are used to illustrate how the measurements compare to those obtained using PVGIS. The difference between the two curves is more than notable for both years. On the one hand, it is due to the fact that the measured values are for specific years (2022, 2023) while the values obtained with PVGIS have been calculated with mean radiation values. To obtain the results of the PV output with PVGIS as has been stated in section 3.8.1 the database used was PVGIS-SARAH2, whose data has been validated with several ground stations.

Having different weather files highlights the impact they have on the results. In the summer months the real solar production is much higher than that simulated with PVGIS, while in the months of November and December it is lower due to the snow deposited on the PV panels.

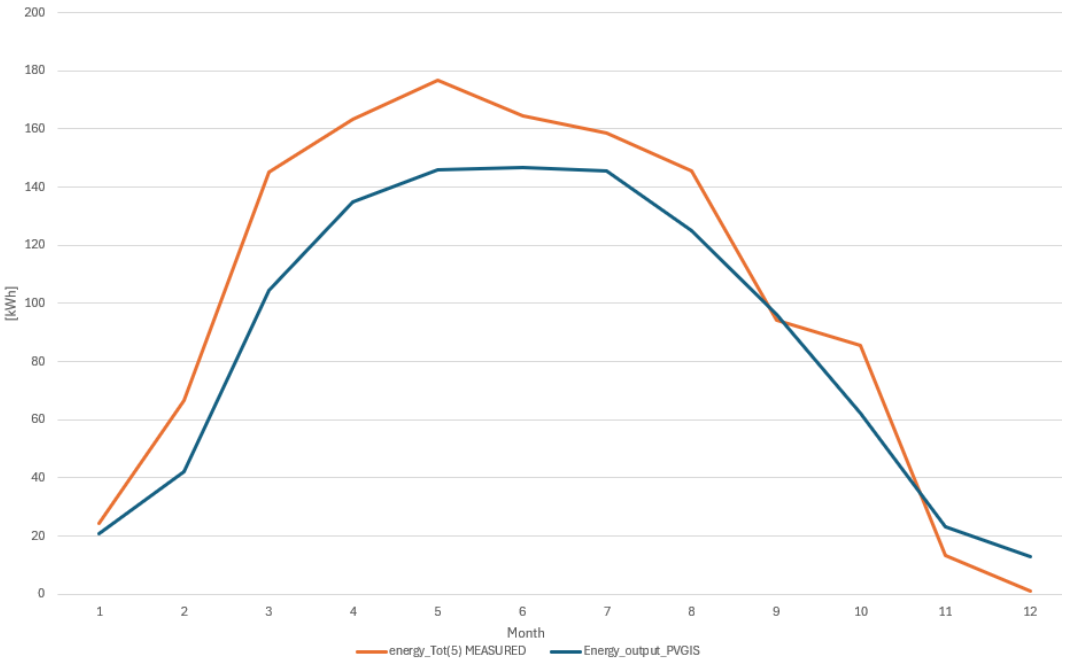

Figure 42 PV output comparison between 1.17 kW PV-system output in building 45 of the HiG and the simulation with PVGIS for 2022

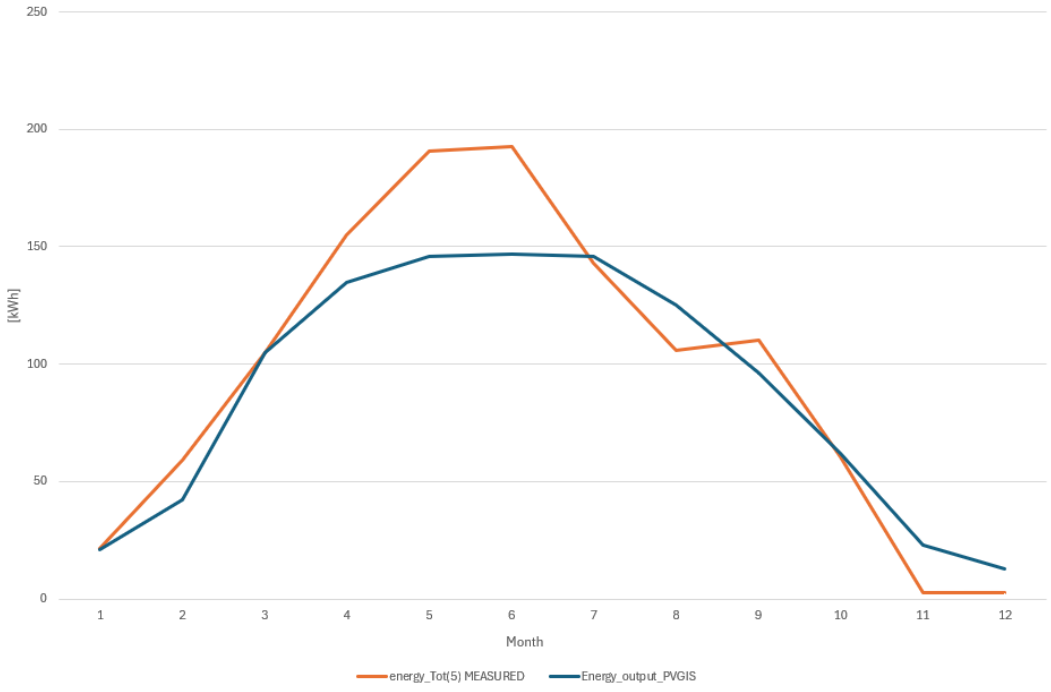

Figure 43 PV output comparison between 1.17 kW PV-system output in building 45 of the HiG and the simulation with PVGIS for 2023

4.1.3 Comparison with STRÅNG data entered into WINSUN program

In order to carry out the following figures (Figure 44 and Figure 45), global radiation and diffuse radiation values obtained from the STRÅNG database have been entered into the WINSUN software. The data presented by the database presented errors on certain days. Radiation values of - 999 W/m^2 were presented on one day in 2022 and on four days in 2023 which was having a major impact on results. After locating the days on which the data were erroneous, it was decided to replace the values for these days with the radiation values collected with the pyranometers in building 45 at HiG. The temperature data introduced has been the one extracted from Gävle's weather station of the SMHI.

In contrast to the curves produced by PVGIS software and although one could think that combining different locations in order to collect data could cause inaccurate results, the curves in Figure 44 and Figure 45are very similar in shape to the measured data. These similarities are due to the fact that the radiation data has been collected every year, so the data entered are those corresponding to the years 2022 and 2023. In the year 2022 the curves are very similar, but it is in 2023 when the data for each month of the year are close to being identical. If it were not for the failures in data collection, one could say that the STRÅNG database is very reliable.

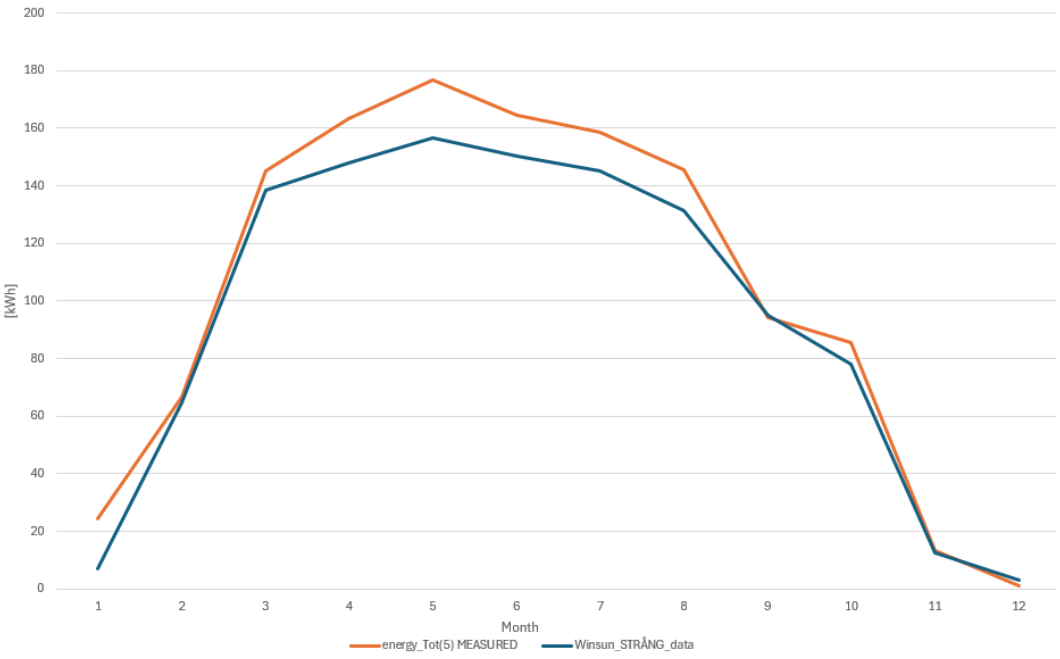

Figure 44 PV output comparison between 1.17 kW PV-system output in building 45 of the HiG and the simulation with STRÅNG data entered into WINSUN for 2022

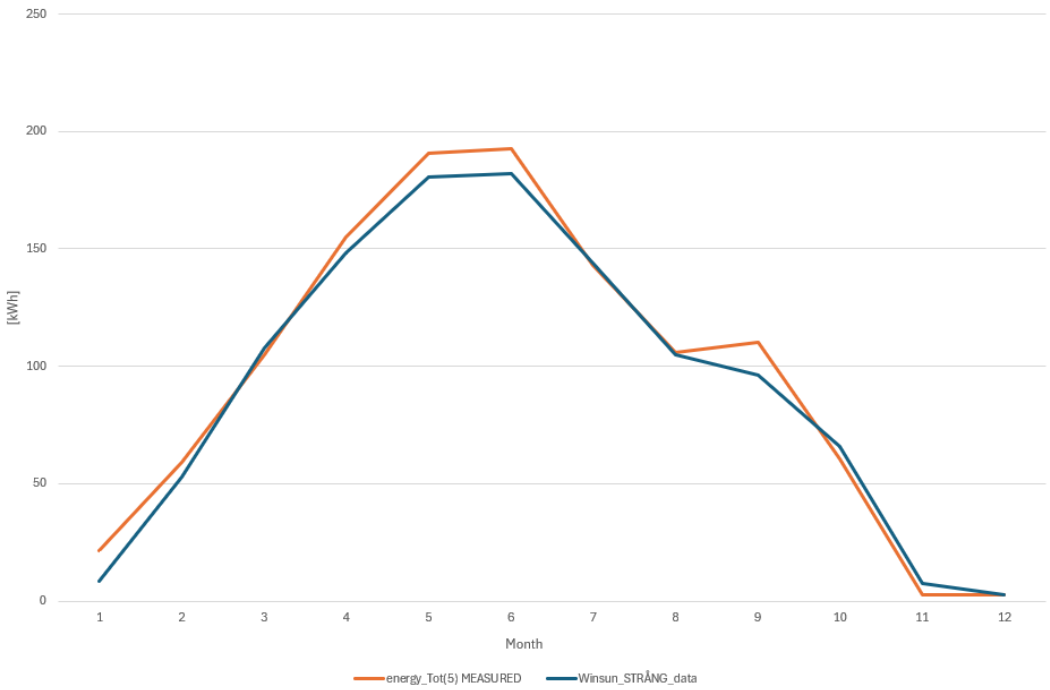

Figure 45 PV output comparison between 1.17 kW PV-system output in building 45 of the HiG and the simulation with STRÅNG data entered into WINSUN for 2023

4.1.4 Comparison with WINSUN website results

Figure 46 and Figure 47 illustrate the curves of the measured data and the results with the WINSUN website having entered the parameters shown in 3.8.3. The file created by WINSUN after inserting the data contains two different curves, one taking into account the horizontal shading and the other one without it. Observing the graphs it can be concluded that not taking into consideration the horizontal shading causes more accurate results in the winter months when the solar altitude (αs) values are lower.

Figure 46 PV output comparison between 1.17 kW PV-system output in building 45 of the HiG and the simulation with WINSUN data for 2022

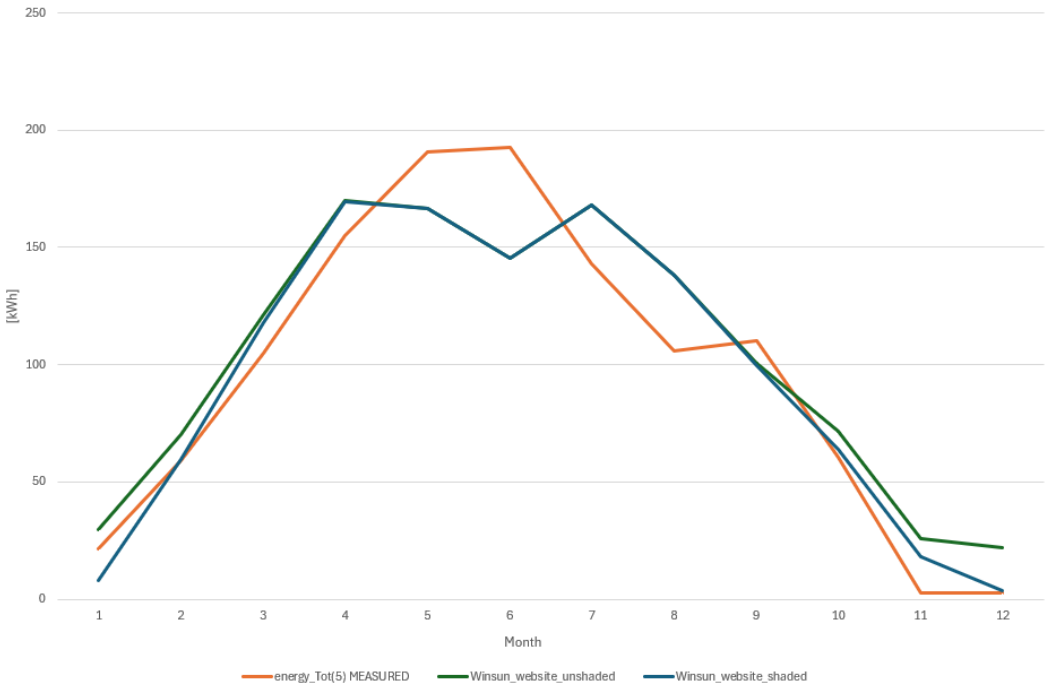

Figure 47 PV output comparison between 1.17 kW PV-system output in building 45 of the HiG and the simulation with WINSUN data for 2023

4.1.5 Statistical errors of the results

Table 6 and Table 7 display the results of the statistical errors between measured and predicted data. As has been explained before, instead of focusing just on one type of statistical error a group of them will be taken into consideration to be able to state with certainty that one model is better than another. Thereby the factor to be taken into account will be the GPI which is a combination of the rest of factors. The calculation model will be more accurate the closer the GPI is to zero.

Table 6 Statistical errors of the estimations of PV solar production in the building 45 of the HiG in 2022

Model	MBD	RMSD	U_{95}	TT	R^2	GPI
PV energy Winsun	1.47%	6.51%	17.83%	0.74%	0.99	8.81E-09
Energy_output_PVGIS	-14.43%	21.07%	51.11%	3.02%	0.96	-1.97E-05
Winsun_STRÅNG_data	-8.74%	11.26%	26.10%	3.95%	0.99	-9.94E-07
Winsun_web_unshaded	-0.77%	12.83%	35.52%	0.19%	0.96	-2.46E-08
Winsun_web_shaded	-6.57%	13.19%	34.23%	1.85%	0.96	-1.99E-06

For the year 2022 Table 6 the best results (GPI = 8.81E-09) have been achieved with the PV energy WINSUN model, with the radiation data collected with the pyranometers, temperature data from SMHI and PV energy production calculated with WINSUN.

Table 7 Statistical errors of the estimations of PV solar production in the building 45 of the HiG in 2023

Model	MBD	RMSD	U_{95}	TT	R^2	GPI
PV energy Winsun	2.85%	6.22%	16.32%	1.79%	0.99	3.09E-08
Energy_output_PVGIS	-7.69%	23.16%	62.41%	1.22%	0.92	-1.03E-05
Winsun_STRÅNG_data	-4.14%	8.12%	21.00%	2.05%	0.99	-1.43E-07
Winsun_web_unshaded	7.04%	23.90%	64.79%	1.07%	0.89	1.23E-05
Winsun_web_shaded	0.78%	22.14%	61.34%	0.12%	0.89	1.41E-07

For the year 2023 (Table 7) the best results (GPI = 3.09E-08) have been achieved with the PV energy WINSUN model again, what makes it the most accurate model.

4.2 Effect of altering the parameters

Once it has been demonstrated how using the presented climate file and entering it into the WINSUN program has provided the most accurate values for the estimation of solar PV production, certain parameters of the input data will be altered, in order to further adjust the results to the real values. The parameters inserted for the first estimation were average values, so there is still room for improvement. The first model will be used as reference and from this the various changes will be made.

Looking one by one at the PV production of the months it has been concluded that the values for the months of January and February should be higher in both 2022 and 2023 and the values for the rest of the months should be slightly lower (Figure 40 and Figure 41).

4.2.1 Effect of the diffuse acceptance coefficient Kd

In the first approximation, the value of Kd = 0.925 has been used, which may be higher than usual. Since for most months the values obtained with WINSUN are higher than those recorded, we will try to reduce this value so that the diffuse radiation portion is reduced and thus the total electrical output. The reduction has been made to Kd = 0.9.

Table 8 and Table 9 show a reduction in Kd has made more accurate the results as it was predicted.

Table 8 Statistical errors of the estimations of PV solar production in the building 45 of the HiG in 2022 changing Kd

Model	MBD	RMSD	U_{95}	TT	R^2	GPI
PV energy Winsun	1.47%	6.51%	17.83%	0.74%	0.99	8.81E-09
PV Winsun (Kd = 0.9)	0.94%	6.27%	17.29%	0.49%	0.99	3.52E-09

Table 9 Statistical errors of the estimations of PV solar production in the building 45 of the HiG in 2023 changing Kd

Model	MBD	RMSD	U_{95}	TT	R^2	GPI
PV energy Winsun	2.85%	6.22%	16.32%	1.79%	0.99	3.09E-08
PV Winsun (Kd = 0.9)	2.27%	5.86%	15.63%	1.46%	0.99	1.79E-08

4.2.2 Effect of the system efficiency

Due to the fact that the elements that are part of the photovoltaic installation have been in operation for several years, their efficiency may have been reduced. Therefore, the system efficiency value will be reduced to 0.9 in order to adjust the values obtained with WINSUN to the measured values.

Table 10 Statistical errors of the estimations of PV solar production in the building 45 of the HiG in 2022 changing system efficiency

Model	MBD	RMSD	U_{95}	TT	R^2	GPI
PV energy Winsun	1.47%	6.51%	17.83%	0.74%	0.99	8.81E-09
System efficiency = 0,9	0.14%	5.87%	16.26%	0.07%	0.99	6.62E-11

Table 11 Statistical errors of the estimations of PV solar production in the building 45 of the HiG in 2023 changing system efficiency

Model	MBD	RMSD	U_{95}	TT	R^2	GPI
PV energy Winsun	2.85%	6.22%	16.32%	1.79%	0.99	3.09E-08
System efficiency = 0,9	1.50%	5.50%	14.96%	0.98%	0.99	7.23E-09

4.2.3 Effect of the horizontal shading

The alteration of the above parameters has been done with the objective of reducing the PV output in most of the months. However, with the change of horizontal shading we will try to increase the PV output in the first months of the year, without increasing it a lot in the rest of the year. The horizontal shading value will be changed from 10º to 7º.

Table 12 and Table 13 illustrate how reducing the horizontal shading, the GPI has increased, what means that the simulation is now less accurate. Nevertheless, the value of the R^2 shows a value of 1.0 meaning that the tendency of the values is the same for both measured and simulated data.

Table 12 Statistical errors of the estimations of PV solar production in the building 45 of the HiG in 2022 changing horizontal shading

Model	MBD	RMSD	U_{95}	TT	R^2	GPI
PV energy Winsun	1.47%	6.51%	17.83%	0.74%	0.99	8.81E-09
Horizontal shading = 7º	4.85%	6.15%	14.14%	4.13%	1.00	6.33E-08

Table 13 Statistical errors of the estimations of PV solar production in the building 45 of the HiG in 2023 changing horizontal shading

Model	MBD	RMSD	U_{95}	TT	R^2	GPI
PV energy Winsun	2.85%	6.22%	16.32%	1.79%	0.99	3.09E-08
Horizontal shading = 7º	5.36%	6.86%	15.84%	4.35%	1.00	1.02E-07

4.2.4 Most accurate model

Observing the results of the previous sections, it can be concluded that mixing the changes of these three parameters, Kd, system efficiency and horizontal shading can make a really accurate model.

A reduction of the horizontal shading mainly increases the results in the months when the altitude values are low, but also increases the PV output in the other months. For this reason, it was decided to use values of Kd = 0.875 and system efficiency = 0.875.

Table 14 and Table 15 show how all the statistical errors show better values than the first approximation, improving a lot the value of the GPI. Moreover, they show how changing the three parameters has caused the best approximation.

Table 14 Statistical errors of the estimations of PV solar production in the building 45 of the HiG in 2022 changing three parameters

Model	MBD	RMSD	U_{95}	TT	R^2	GPI
PV energy Winsun	1.47%	6.51%	17.83%	0.74%	0.99	8.81E-09
All measures 0,875/0,875/7º	-0.41%	4.31%	11.93%	0.31%	1.00	-2.70E-10

Table 15 Statistical errors of the estimations of PV solar production in the building 45 of the HiG in 2023 changing three parameters

Model	MBD	RMSD	U_{95}	TT	R^2	GPI
PV energy Winsun	2.85%	6.22%	16.32%	1.79%	0.99	3.09E-08
All measures 0,875/0,875/7º	-0.02%	5.48%	15.18%	0.01%	1.00	-1.06E-12

Figure 48 and Figure 49 depict both measured values of PV output and simulated PV output with WINSUN after adjusting the parameters, horizontal shading, Kd and system efficiency. It represents the most accurate approximation.

Figure 48 Comparison between measured and simulated data after adjusting parameters 2022

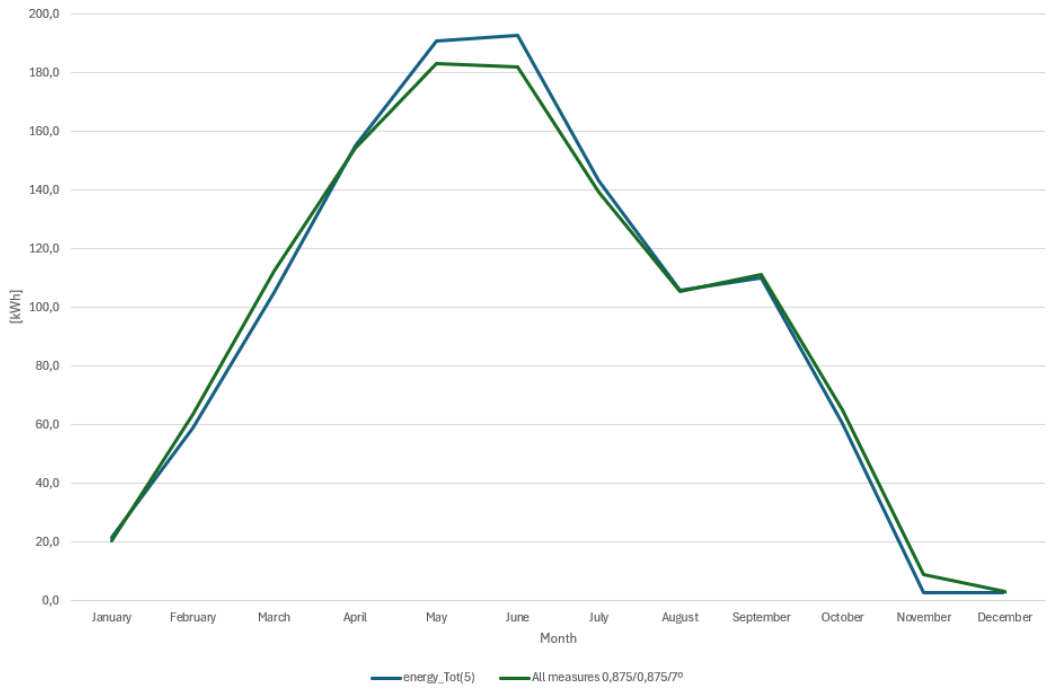

Figure 49 Comparison between measured and simulated data after adjusting parameters 2023

4.3 Overall results

Table 16 and Table 17 illustrate some of the main results of the analysis done in this project. It can be observed how the diffuse horizontal radiation has been corrected and the similarities between measured and the simulated data in terms of radiation and PV production.

Table 16 Overall results for 2022

Month	Measured global horizontal [kWh/m²]	Measured diffuse horizontal [kWh/m2]	Corrected diffuse horizontal [kWh/m2]	Measured global 45°/-12,5° [kWh/m2]	Simulated global 45° south [kWh/m2]	Measured PV-electricity [kWh/kWp]	Simulated PV-electricity [kWh/kWp]
January	9.86	5.19	5.13	28.21	20.89	20.89	18.06
February	30.38	23.57	12.49	68.46	72.70	56.78	61.48
March	84.25	29.56	25.01	147.22	156.48	124.15	127.94
April	131.08	43.11	40.52	167.55	172.82	139.41	138.43
May	172.37	59.22	56.12	185.26	186.13	151.15	145.38
June	178.54	62.59	58.63	176.28	176.64	140.51	134.34
July	166.43	66.46	60.74	168.78	170.57	135.61	130.08
August	132.92	59.54	47.07	154.64	159.27	124.27	119.87
September	73.08	37.82	33.33	97.85	104.15	80.59	82.62
October	43.76	19.89	17.91	86.74	93.27	73.14	76.21
November	8.96	7.77	6.59	15.94	15.80	11.23	13.20
December	5.52	5.51	4.13	14.48	3.26	1.07	2.79
Total	1037.17	420.25	367.68	1311.43	1331.98	1058.79	1050.38

Table 17 Overall results for 2023

Month	Measured global horizontal [kWh/m²]	Measured diffuse horizontal [kWh/m2]	Corrected diffuse horizontal [kWh/m2]	Measured global 45º/-12,5º [kWh/m2]	Simulated global 45º south [kWh/m2]	Measured PV-electricity [kWh/kWp]	Simulated PV-electricity [kWh/kWp]
January	10.72	9.43	7.31	24.09	20.17	18.54	17.35
February	28.09	13.69	12.64	62.63	63.46	50.40	53.94
March	72.33	46.00	29.49	109.30	115.73	89.74	95.73
April	120.91	36.39	33.71	158.27	164.11	132.59	131.27
May	186.29	51.99	49.55	203.44	201.77	162.95	155.64
June	205.41	57.96	55.65	207.62	203.83	164.54	154.71
July	152.84	59.74	58.13	154.67	155.20	122.26	118.66
August	101.32	53.37	49.88	111.83	115.82	90.24	89.76
September	81.98	42.62	35.76	115.68	121.11	94.10	94.82
October	35.75	19.65	17.07	63.10	67.41	51.56	55.52
November	6.95	6.52	6.09	9.36	8.73	2.26	7.55
December	4.22	4.01	2.98	12.77	3.05	2.38	2.63
Total	1006.79	401.38	358.26	1232.75	1240.39	981.54	977.59

4.4 Different factors influencing the PV performance

4.4.1 Influence of the snow in the PV performance

As the study was carried out in a Nordic country, specifically Sweden, it is important to emphasize the influence of snow on the performance of solar panels. Figure 50 illustrates both snow depth and PV output of the solar panels for years 2022 and 2023. Snow has a lot of influence in the performance of the PV panels owing to the fact that it covers the solar panel disabling them to receive the total radiation available. The worst years for PV production are November and December. In these months the effects of the snow and the low number of hours of sunlight reduce production.

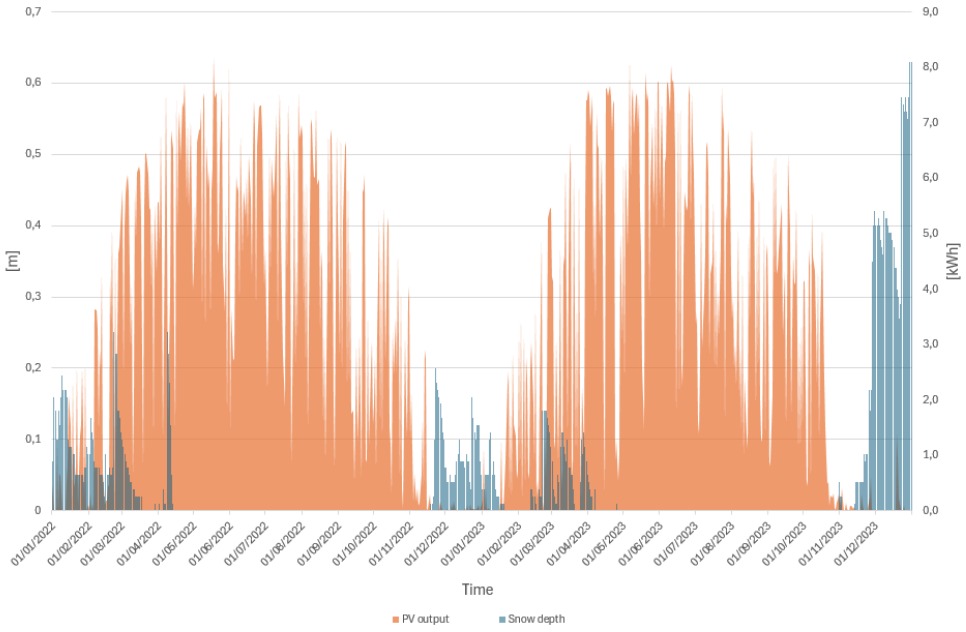

Figure 50 Snow depth and PV output representation for years 2022 and 2023

With Figure 50 is difficult to evaluate the effect that the snow has in the PV output, owing to the lack of radiation information. Apart from the snow depth and the PV output Figure 51 also illustrates the daily radiation received in the building 45 of HiG with a tilt of 45° with an azimuth of -12.5°. Figure 51 shows how snow mainly reduces the PV output with respect to the radiation received in the months of November and December. Despite the fact that from January to May there is still snow, the performance of the solar panels is less affected by it.

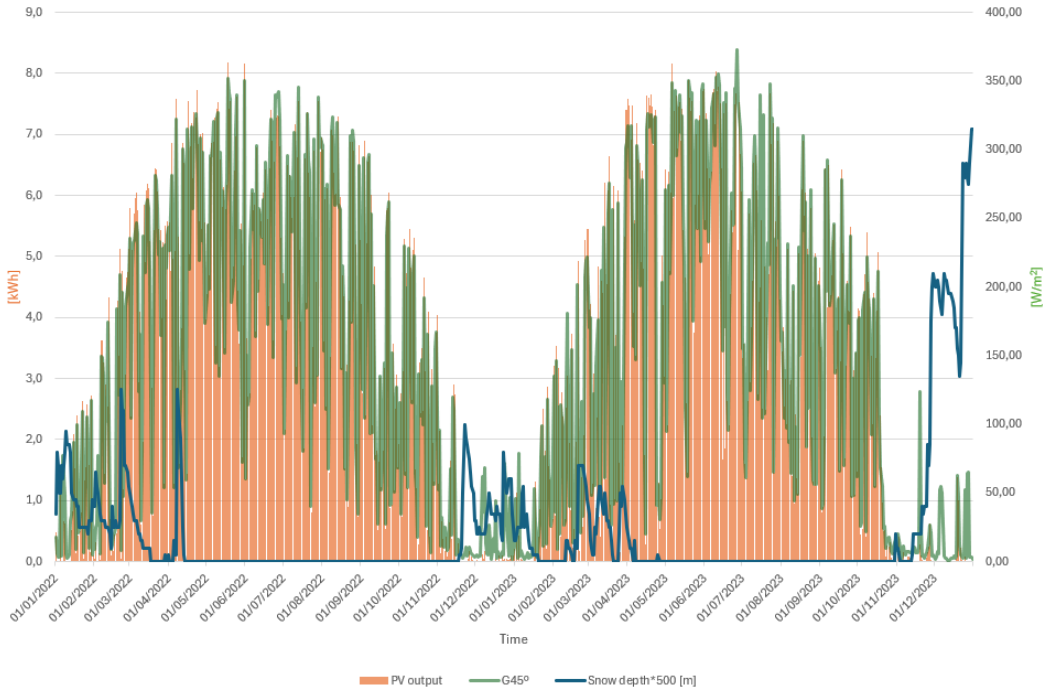

Figure 51 Snow depth and PV output representation together with total radiation with a $\beta = 45°$ for years 2022 and 2023

As can be seen in Figure 52, there are sometimes in which panels are partially covered. In these cases, PV output is partially reduced but not completely.

Figure 52 Solar panels covered by snow in the PV system of HiG

5 Discussions

The primary objective of this study, which was to create a climate archive to facilitate the estimation of solar PV production, has been successfully achieved. Total radiation data, temperature data, and diffuse radiation data have been obtained and adjusted.

In order to validate this climate file, temperature data had to be extracted at the studied location and data from three different pyranometers had to be extracted. The problem was that there were times when the horizontal diffuse radiation did not present real values because the ring had not been correctly positioned to shade the radiation sensor and receive only diffuse radiation. Using the radiation data from *Pyranometer 1*, *Pyranometer 2* and Eq. 24, actual horizontal diffuse radiation data were obtained.

In contrast to other studies that attempted to determine diffuse radiation by means of mathematical models (Jamil & Akhtar, 2017; Torres et al., 2010) , using experimental data to create and validate them, in the case studied it was decided to combine data extracted directly from measured horizontal diffuse radiation with calculated data. It is possible that the method chosen for the determination of $G_{d.h}$ may not have been the most accurate, given that in some months the data have shown more accurate data with unaltered $G_{d.h}$ data. However, in general, the results are improved when the $G_{d.h}$ values are adjusted.

Since some data has been interpolated (temperature and radiation at certain hours), the results are not exactly what you would expect, but are close enough to validate them. Figure 29 and Figure 35 show a much more realistic shape of the curves for G_h. $G_{d.h}$. $G_{b.h}$ values. Another factor that could have affected the results is the years that the devices of the PV system (inverter, solar panels, cables) have been functioning. However, Figure 36 and Figure 37 in section 3.6 illustrate how the pyranometers used and the simulation program WINSUN show similar results despite the inaccuracy in some of the winter months due to the horizontal shading value set as input, which has been later adjusted.

The comparison between the data developed in this thesis and data coming from different databases and PV calculator software such as PVGIS, STRÅNG and WINSUN website has allowed to present the results as the most accurate for the location studied.

Graphical comparisons have been of great help, however, the use of statistical error analysis has allowed the study of the accuracy of the data to be improved. Values of the rMBE or MBD (calculated in percentage) better than the ones obtained in the study carried out by (Olczak, 2022) from 0 to 8% have been obtained. In the studied case MBD have oscillated were 1.47% for 2022 and 2.85% for 2023 and after the parameter adjustments they have ended up being -0.41% and -0.02% respectively. This can be due to the distance of 10 km between the pyranometer and the place of the PV panels in Olczak's study.

The implementation of the GPI used in the works (Behar et al., 2015; Jamil & Akhtar, 2017) as a statistical method to determine the precision errors has been of great help in confirming the validation of the data and allowing the accurate adjustment of the parameters. On the other hand, these parameters have been adjusted considering the results and observing the trend of the curves that can be seen in Figure 38 and Figure 39. Therefore, the parameter settings may not have been as accurate as possible. For future studies, models could be run to determine what the values of these parameters should be at the site studied.

It would be interesting for future studies to have valid data of diffuse radiation measured over several years in order to be able to make predictive models similar to the one of (Jamil & Akhtar, 2017). Therefore, there would not be the necessity of moving the shading ring frequently, saving work and increasing the reliability of the results. This would make it possible to get a especially accurate climate file for the city of Gävle.

6 Conclusions

6.1 Study results

Among the main results obtained in this project is the estimation of the horizontal diffuse radiation by means of different adjustments considering the erroneous and correct values of radiation received with the *pyranometer 3* (pyranometer with the shading ring). Most of the values were correct, but there were some erroneous values, which were corrected by means of Eq. 24. This equation considers the values obtained by the other two pyranometers of the installation, *pyranometer 1* and *pyranometer 2*, which are responsible for recording the global radiation at $\beta = 45^{\circ}$ and $\gamma = -12.5^{\circ}$ and the horizontal global radiation, respectively.

It is complicated, but it is possible to generalize the method to estimate the $G_{d.h}$ of this project for different studies, because measured and calculated data have been used at the same time. The problem with this method lies in the failures in the recording of diffuse radiation data. In addition, when the denominator of Eq. 24 gives results close to zero, giving very large $G_{d.h}$ results, another estimation method should be sought.

Entering the climate file generated in the WINSUN program we have obtained values very similar to those of the PV energy obtained by the system of 1.17 kWp as can be seen in the following section 4.2.4.

The most accurate estimation was achieved after adjusting the values of system efficiency, K_d and horizontal shading. If the system efficiency value is reduced, all monthly PV output values are reduced in the same proportion. If the value of K_d is reduced, the months in which the proportion of diffuse radiation received is higher are the months in which the PV output will show proportionally lower values. On the other hand, reducing the horizontal shading angle causes the PV output to be higher in these winter months.

Comparing the radiation data received with the pyranometers, it shows higher percentage values in the months when snow precipitation is frequent with respect to the energy produced by the panels. This indicates the influence of snow, since the pyranometers have been cleaned more frequently than the panels. However, the frequency of cleaning is unknown, so the influence of the snow on the PV performance output cannot be determined in this case.

6.2 Outlook

As has been stated in section 5 it would be interesting to make a predictive model for diffuse radiation to be able to have a more precise climate file. Another topic of research would be to adjust the parameters inserted in WINSUN for a particular PV system to be able to accurately determine the PV output based on these parameters.

Moreover, it would also be worth evaluating the influence of snow precipitation in this location, as the Nordic countries are generally associated with high snow precipitation which can cause low PV panel yields. However, these are countries where during the summer the daylight hours soar, leading the PV panels to produce a large amount of energy in these months.

The main objective, which was to obtain the most accurate climate file for the city of Gävle, has been achieved. It will be provided to the University of Gävle to be made available to any individual who wishes to study the possibility of any type of photovoltaic installation. Whether for industrial buildings, office buildings or single-family houses. The WINSUN program together with the climate file will provide accurate values of generated electrical PV power.

6.3 Perspectives

Setting this work in a broader view of energy systems and sustainability, it can be said that it will facilitate and promote PV installations in the city of Gävle. reducing the emissions produced by non-renewable energy generation. In addition, the installation of PV panels can also encourage people to purchase electric vehicles because a PV installation allows to produce electric energy at a low price considering only the installation costs and low maintenance costs. Moreover, it will help the visibility of PV energy in a country where this technology is not very common but has great potential.

This study aligns with some of the Global Goals, (7^{th} affordable and clean energy) providing cheap clean energy to the individuals making PV installations, (8^{th} decent work and economic growth) enhancing the economic growth of sustainable companies in charge of building PV installations, (11^{th} sustainable cities and communities) fostering to build more PV installations what will make cities and communities less dependent on electricity prices and more sustainable and (13^{th} climate action) reducing CO_2 emissions.

References

99% efficiency 80A 100A MPPT solar charge controller 48V/96V. (2019). Retrieved April 16, 2024, from https://milesolar.com/products/38/80a-100a-48v-96v-mppt-solar-charge-controller-80amp-100amp

Behar, O., Khellaf, A., & Mohammedi, K. (2015). Comparison of solar radiation models and their validation under Algerian climate - The case of direct irradiance. *Energy Conversion and Management*, *98*, 236–251. https://doi.org/10.1016/j.enconman.2015.03.067

Björn O Karlsson. (2022). *Energy resources-HiG, 2022 Solar radiation*.

Björn O Karlsson. (2022). *Solar angles - Renewable energy resources University of Gavle*.

CR1000: Measurement and Control Datalogger. (2007). Retrieved April 27, 2024, from https://www.campbellsci.com/cr1000

Despotovic, M., Nedic, V., Despotovic, D., & Cvetanovic, S. (2015). Review and statistical analysis of different global solar radiation sunshine models. In *Renewable and Sustainable Energy Reviews* (Vol. 52, pp. 1869–1880). Elsevier Ltd. https://doi.org/10.1016/j.rser.2015.08.035

Drummond, A. J. (1956). *On the Measurement of Sky Radiation*.

Duffie, J. A., Beckman, W. A., & Blair, N. (2020). *Solar engineering of thermal processes : photovoltaics and wind*.

Formolli, M., Lobaccaro, G., & Kanters, J. (2021). Solar energy in the nordic built environment: Challenges, opportunities and barriers. In *Energies* (Vol. 14, Issue 24). MDPI. https://doi.org/10.3390/en14248410

Franklin, E. (2018). *Solar Photovoltaic (PV) System Components*.

Gaikwad, Mr. K. L. (2020). Materials for Solar Energy. *International Journal for Research in Applied Science and Engineering Technology*, *8*(8), 827–830. https://doi.org/10.22214/ijraset.2020.31036

Ground Static Mounting System for Solar Panels SMS-402 by SolarSK. (n.d.). Retrieved April 16, 2024, from https://solarssk.com/solar-ground-mounting-systems/static-ground-mount-system-sms-402/

Gueymard, C. A. (2014). A review of validation methodologies and statistical performance indicators for modeled solar radiation data: Towards a better bankability of solar projects. In *Renewable and Sustainable Energy Reviews* (Vol. 39, pp. 1024–1034). Elsevier Ltd. https://doi.org/10.1016/j.rser.2014.07.117

Innovation: Thin Film Solar Cells at MX2016 - MaterialDistrict. (2016). Retrieved April 17, 2024, from https://materialdistrict.com/article/innovation-thin-film-solar-cells-at-mx2016/

IV Curve | PVEducation. (2019). Retrieved April 27, 2024, from https://www.pveducation.org/pvcdrom/solar-cell-operation/iv-curve

Jamil, B., & Akhtar, N. (2017). Estimation of diffuse solar radiation in humid-subtropical climatic region of India: Comparison of diffuse fraction and diffusion coefficient models. *Energy*, *131*, 149–164. https://doi.org/10.1016/j.energy.2017.05.018

'Jenkins, N., & 'Ekanayake, J. (2017). *Renewable Energy Engineering* (1st ed., Vol. 1). University Printing House.

JRC Photovoltaic Geographical Information System (PVGIS) - European Commission. (2022). Retrieved May 6, 2024, from https://re.jrc.ec.europa.eu/pvg_tools/en/tools.html

Karlsson, B. (2022). *2022-11-23, Energy resources Calculation of the Performance of a PV-system in Winsun*.

Kudusov, M. A., Madvaliev, U., & Elistratov, V. V. (2021). Evaluation of the Efficiency of Already Existing Network Solar Photovoltaic Plants Operating 24/7/365 in Low-Voltage Power Supply Systems of Social Facilities in the City of Dushanbe. *Applied Solar Energy (English Translation of Geliotekhnika)*, *57*(4), 323–332. https://doi.org/10.3103/S0003701X21040071

Ladda ner meteorologiska observationer | SMHI. (n.d.). Retrieved April 27, 2024, from https://www.smhi.se/data/meteorologi/ladda-ner-meteorologiska-observationer/#param=airtemperatureInstant,stations=core

Monocrystalline Solar Cell and its efficiency - SolarSena. (n.d.). Retrieved April 17, 2024, from https://solarsena.com/monocrystalline-solar-cells-explained/

Nabipour Afrouzi, H., Vahabi Mashak, S., Abdul-Malek, Z., Mehranzamir, K., & Salimi, B. (2013). Solar array and battery sizing for a photovoltaic building in Malaysia. *Jurnal Teknologi (Sciences and Engineering)*, *64*(4), 79–84. https://doi.org/10.11113/jt.v64.2106

Olczak, P. (2022). Comparison of modeled and measured photovoltaic microinstallation energy productivity. *Renewable Energy Focus* , *43*, 246–254. https://doi.org/10.1016/j.ref.2022.10.003

P Type Polycrystalline Silicon Solar Cell - China Polycrystalline Silicon and Poly Cell. (2019). Retrieved April 17, 2024, from https://dsnewenergy.en.made-in-china.com/product/MOwxcVkJCQWi/China-P-Type-Polycrystalline-Silicon-Solar-Cell.html

Patel, M. R. (1999). *Wind and solar power systems*. CRC Press.

PVGIS data sources &calculation methods - European Commission. (2020). Retrieved May 6, 2024, from https://joint-research-centre.ec.europa.eu/photovoltaic-geographical-information-system-pvgis/getting-started-pvgis/pvgis-data-sources-calculation-methods_en

¿Qué es la energía fotovoltaica? - APPA Renovables. (n.d.). Retrieved April 15, 2024, from https://www.appa.es/appa-fotovoltaica/que-es-la-energia-fotovoltaica/?cn-reloaded=1

Rezvani, M., Gholami, A., Gavagsaz-Ghoachani, R., Phattanasak, M., & Zandi, M. (2022). A review of the factors affecting the utilization of solar photovoltaic panels. *Proceedings - 2022 Research, Invention, and Innovation Congress: Innovative Electricals and Electronics, RI2C 2022*, 62–69. https://doi.org/10.1109/RI2C56397.2022.9910278

Ruan, T., Wang, F., Topel, M., Laumert, B., & Wang, W. (2024). A new optimal PV installation angle model in high-latitude cold regions based on historical weather big data. *Applied Energy*, *359*. https://doi.org/10.1016/j.apenergy.2024.122690

SMA Energy Meter EMETER-20 | mg-solar-shop. (2020). Retrieved April 16, 2024, from https://www.mg-solar-shop.com/pv-monitoring/sma-energy-meter-emeter-20.html

Solar - IEA. (2023). Retrieved April 15, 2024, from https://www.iea.org/energy-system/renewables/solar-pv

Solar Combiner Box PV Combiner Box 4 String With15A Palestine | Ubuy. (2018). Retrieved April 16, 2024, from https://www.ubuy.com.ps/en/product/1YPVMISK-polyenergy-pv-combiner-box-4-stringwith15a-rated-current-fuse-63a-solar-dc-breaker-lightning-arreste

Solar Inverters | SMA Solar. (n.d.). Retrieved April 16, 2024, from https://www.sma.de/en/products/solar-inverters

Solar Panel Mounting Systems: Types and Considerations for Installers. (2023). Retrieved April 16, 2024, from https://arka360.com/ros/solar-panel-mounting-systems-installers/

Solar Technology, S. A. (n.d.). *Sunny Boy 1200 / 1700 / 2500 / 3000*. www.SMA-Solar.com

Stone, R. J. (1993). IMPROVED STATISTICAL PROCEDURE FOR THE EVALUATION OF SOLAR RADIATION ESTIMATION MODELS. In *Solar Energy* (Vol. 5, Issue 4).

STRÅNG. (2006). Retrieved May 6, 2024, from https://strang.smhi.se/

Torres, J. L., De Blas, M., García, A., & de Francisco, A. (2010). Comparative study of various models in estimating hourly diffuse solar irradiance. *Renewable Energy*, *35*(6), 1325–1332. https://doi.org/10.1016/j.renene.2009.11.025

Types of Solar Panels: Types, Working, Application with (PDF). (2022). Retrieved April 17, 2024, from https://www.theengineerspost.com/solar-panel-types/?utm_content=cmp-true

What is a combiner box? (2015). Retrieved April 16, 2024, from https://www.solarpowerworldonline.com/2015/06/what-is-a-combiner-box/

Yang, Y., Campana, P. E., Stridh, B., & Yan, J. (2020). Potential analysis of roof-mounted solar photovoltaics in Sweden. *Applied Energy*, *279*. https://doi.org/10.1016/j.apenergy.2020.115786

Appendix A

EOPLLY NEW ENERGY TECHNOLOGY CO., LTD

optimized photovoltaic solution

EOPLLY

EOPLLY 125M / 72 (190-200W)

Monocrystalline Solar Module

EOPLLY 125 Monocrystalline series solar modules are made of 72 pcs 125× 125mm monocrystalline solar cells in series with high efficency, high transmission rate and low iron tempered glass, anti-aging EVA and high flame resistant back sheet, and anodized aluminum alloy. The modules have advantages of high efficiency, long service life, easy to install as well as high wind and hail impact resistance.

Features and Benefits

- Member of PV CYCLE
- Pass 5400 Pa Pressure Test
- High efficiency Outstanding low-light performance
- 10 years product guarantee
- Power warranties: 10 years (90%), 25 years (80%)
- Applicable for on-grid and 24V off-grid system
- Power tolerance +/-3% Three bypass diodes

Electrical Specifications

Type / Model	125M/72-190	125M/72-195	125M/72-200
open circuit voltage Voc(V)	44.90	45.20	45.40
optimum operating voltage Vmp(V)	37.08	37.70	37.90
short-circuit current Isc(A)	5.55	5.57	5.59
optimum operating current Imp(A)	5.15	5.21	5.25
maximum power at STC Pmax	190W	195W	200W
module effciency	14.88%	15.27%	15.67%
operating temperature	-40℃ to 85℃	-40℃ to 85℃	-40℃ to 85℃
maximum system voltage	1000V	1000V	1000V
pressure resistance	227g steel ball falls down from 1m height under 60m/s wind		

The electrical specifications are typical average value from historical production data.
The electrical data relates to standard test conditions [STC]: 1,000W/m² ; AM 1.5; 25°C

EOPLLY 125M / 72 (190-200W)

Monocrystalline Solar Module

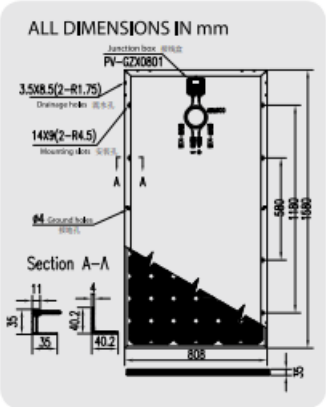

Mechanical Characteristics

Solar Cell	Monocrystalline silicon solar cell 125x125(mm)
No.of Cells	72 (6x12)
Dimensions	1580x808x35(mm)
Weight	15kg
Front Glass	3.2mm (0.13 inches) tempered glass
Frame	Anodized aluminum alloy

Output

Cable Type	Φ=4mm²
Lengths	L=900mm
Junction Box	PV-GZX0801MC4
Over-current protection rating[A] : 10A	

Temperature Coefficients

Nominal Operating Cell Temperature (NOCT)	47±3°C
Temperature Coefficient of Pmax	-0.4459%/°C
Temperature Coefficient of Voc	-0.3882%/°C
Temperature Coefficient of Isc	0.0625%/°C

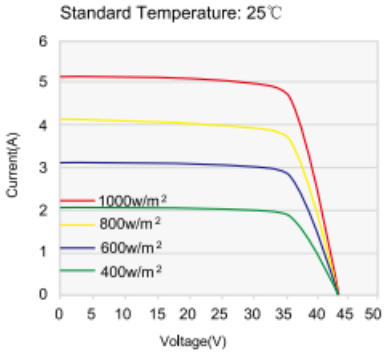

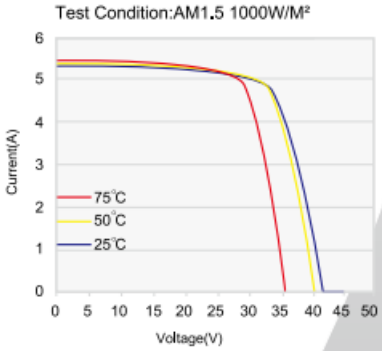

ecodirect

Safe
- Integrated ESS DC switch-disconnector
- Galvanic isolation

All purpose
- For indoor and outdoor installation
- Suitable for generator grounding

Reliable
- Tried and tested technology
- Maintenance free, thanks to convection cooling

Simple
- DC plug system SUNCLIX

SUNNY BOY 1200 / 1700 / 2500 / 3000

Proven technology for secure investments

Universally applicable: the Sunny Boy inverters 1200, 1700, 2500 and 3000 are used in the most diverse AC grids thanks to their galvanic isolation. In addition, the devices are suitable for simple grounding of the generator. Their integrated ESS DC switch-disconnector makes installation simpler while also reducing assembly costs. Equipped with the OptiTrac MPP-tracking process, it will always find the best working point, even under dynamic weather conditions. In this way, it reliably converts solar energy into solar yield.

Technical data	Sunny Boy 1200	Sunny Boy 1700	Sunny Boy 2500	Sunny Boy 3000
Input (DC)				
Max. DC power (@ cos φ = 1)	1320 W	1850 W	2700 W	3200 W
Max. DC voltage	400 V	400 V	600 V	600 V
MPP voltage range	100 V – 320 V	147 V – 320 V	224 V – 480 V	268 V – 480 V
DC nominal voltage	120 V	180 V	300 V	350 V
Min. DC voltage / start voltage	100 V / 120 V	139 V / 180 V	224 V / 300 V	268 V / 330 V
Max. input current / per string	12.6 A / 12.6 A	12.6 A / 12.6 A	12 A / 12 A	12 A / 12 A
Number of MPP trackers / strings per MPP tracker	1 / 2	1 / 2	1 / 3	1 / 3
Output (AC)				
AC nominal power (@ 230 V, 50 Hz)	1200 W	1550 W	2300 W	2750 W
Max. AC apparent power	1200 VA	1700 VA	2500 VA	3000 VA
Nominal AC voltage; range	220, 230, 240 V; 180 V – 265 V	220, 230, 240 V; 180 V – 265 V	220, 230, 240 V; 180 V – 265 V	220, 230, 240 V; 180 V – 265 V
AC grid frequency; range	50, 60 Hz; ± 4.5 Hz	50, 60 Hz; ± 4.5 Hz	50, 60 Hz; ± 4.5 Hz	50, 60 Hz; ± 4.5 Hz
Max. output current	6.1 A	8.6 A	12.5 A	15 A
Power factor (cos φ)	1	1	1	1
Phase conductors / connection phases	1 / 1	1 / 1	1 / 1	1 / 1
Efficiency				
Max. efficiency / Euro-eta	92.1 % / 90.9 %	93.5 % / 91.8 %	94.1 % / 93.2 %	95.0 % / 93.6 %
Protection devices				
DC reverse-polarity protection	●	●	●	●
ESS switch-disconnector	●	●	●	●
AC short circuit protection	●	●	●	●
Ground fault monitoring	●	●	●	●
Grid monitoring (SMA Grid Guard)	●	●	●	●
Galvanically isolated / all-pole sensitive fault current monitoring unit	●/–	●/–	●/–	●/–
Protection class / overvoltage category	I / III	I / III	I / III	I / III
General data				
Dimensions (W / H / D) in mm	440 / 339 / 214	440 / 339 / 214	440 / 339 / 214	440 / 339 / 214
Weight	23 kg	25 kg	28 kg	32 kg
Operating temperature range	-25 °C ... +60 °C	-25 °C ... +60 °C	-25 °C ... +60 °C	-25 °C ... +60 °C
Noise emission (typical)	≤ 41 dB(A)	≤ 46 dB(A)	≤ 33 dB(A)	≤ 30 dB(A)
Internal consumption (night)	< 0.1 W	< 0.1 W	< 0.25 W	< 0.25 W
Topology	LF transformer	LF transformer	LF transformer	LF transformer
Cooling concept	Convection	Convection	Convection	Convection
Electronics protection rating / connection area (as per IEC 60529)	IP65 / IP65	IP65 / IP65	IP65 / IP65	IP65 / IP65
Climatic category (per IEC 60721-3-4)	4K4H	4K4H	4K4H	4K4H
Features				
DC connection: SUNCLIX	●	●	●	●
AC connection: screw terminal / plug connector / springtype terminal	–/●/–	–/●/–	–/●/–	–/●/–
Display: text line / graphic	●/–	●/–	●/–	●/–
Interfaces: RS485 / Bluetooth®	o/o	o/o	o/o	o/o
Warranty: 5 / 10 / 15 / 20 / 25 years	●/o/o/o/o	●/o/o/o/o	●/o/o/o/o	●/o/o/o/o
Certificates and permits (more available on request)	CE, VDE 0126-1-1, UTE C 15-712-1, DK 5940*, RD 1663, G83/1-1, CER/06/190 (only SB 1700), PPC, AS4777, EN 50438**, C10/C11, PPDS, IEEE 929		CE, VDE 0126-1-1, DK 5940*, RD 1663, G83/1-1, CER/06/190, PPC, AS4777, EN 50438**, C10/C11, PPDS	
*Only applies to IT variants, ** Does not apply to all national deviations of EN 50438				
● Standard features o Optional features – not available Data at nominal conditions				
Type designation	SB 1200	SB 1700	SB 2500	SB 3000

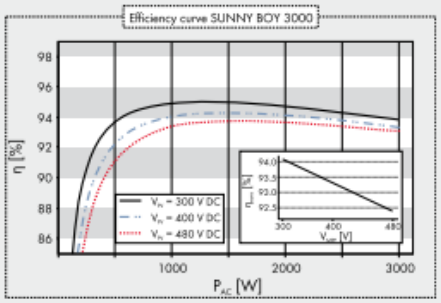

Accessories

RS485 interface of type 485PB-NR

Bluetooth® Piggy Back BTPBINV-NR

Grounding set "Positive" ESHV-P-NR

Grounding set "Negative" ESHV-P-NR

Appendix B

Mean values

For the following equations it is important to know that m_i values represent the measured values and c_i values represent the predicted ones.

$$\bar{m} = \left(\frac{1}{n}\right) * \sum_{i=1}^{n} m_i \qquad \textit{Eq. 27}$$

$$\bar{c} = \left(\frac{1}{n}\right) * \sum_{i=1}^{n} c_i \qquad \textit{Eq. 28}$$

Mean Bias Difference (MBD)

The models that represent the closest value to zero of the MBD will be the most accurate ones. One of the weaknesses of this statistic method is that positive and negative values for the difference between measured and predicted values can be compensated.

$$MBD = \left(\frac{1}{n\bar{m}}\right) * \sum_{i=1}^{n} (c_i - m_i) \qquad \textit{Eq. 29}$$

Root Mean Square Difference (RMSD)

The RMSD represents a little bit better the error since the highlighted weakness of the previous method does not affect it. The lower this value. the more accurate the estimation will be.

$$RMSD = \left(\frac{1}{\bar{m}}\right) * \sqrt{\frac{1}{n} * \sum_{i=1}^{n} (c_i - m_i)^2} \qquad \textit{Eq. 30}$$

Coefficient of determination (R^2)

A value of R^2 close to one represents a more accurate estimation of the values.

$$R^2 = \left(\frac{\sum_{i=1}^{n}(m_i - \bar{m}) * (c_i - \bar{c})}{\sqrt{\sum_{i=1}^{n}(m_i - \bar{m})^2 \sum_{i=1}^{n}(c_i - \bar{c})^2}}\right)^2 \qquad \textit{Eq. 31}$$

Expanded uncertainty (U_{95})

Expanded uncertainty with 95% of confidence level. SD represents the percentage of standard deviation of the difference between measured and predicted data.

$$U_{95} = 1.96 * \sqrt{(SD^2 + RMSD^2)} \qquad \textit{Eq. 32}$$

Standard deviation in percentage.

$$SD = \left(\frac{1}{n\overline{m}}\right) * \sqrt{\sum_{i=1}^{n} n * (c_i - m_i)^2 - \sum_{i=1}^{n} (c_i - m_i)^2} \qquad \textit{Eq. 33}$$

T-statistic test (TT)

The best estimation corresponds to the closest values to zero.

$$TT = \left(\frac{1}{\overline{m}}\right) * \sqrt{((n-1) * MBE^2)/(RMSD^2 - MBE^2)} \qquad \textit{Eq. 34}$$

Global Performance Indicator (GPI)

The GPI is a combination of different statistical methods created to evaluate the best estimation of the data. All the values are introduced as percentages and the closer the value of the GPI to zero the better the estimations will be.

$$GPI = MBD * RMSD * U_{95} * TT * (1 - R^2) \qquad \textit{Eq. 35}$$